Cell Reports

Atoh1 Directs Regeneration and Functional Recovery of the Mature Mouse Vestibular System

Graphical Abstract

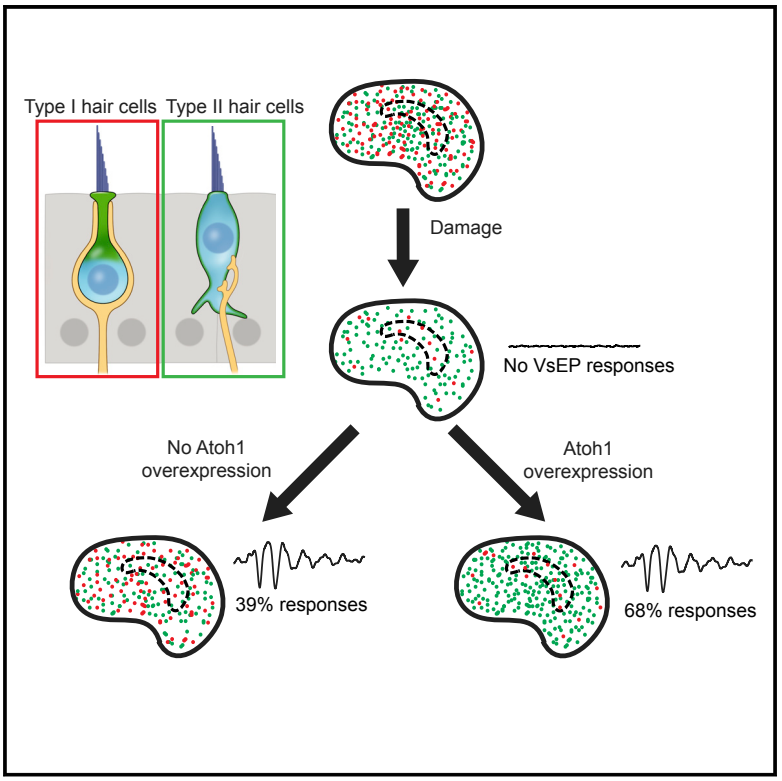

Highlights

- The mature mouse utricle spontaneously regenerates hair cells and recovers function
- Regenerated hair cells gradually increase and acquire bundles over months
- Atoh1 overexpression enhances proliferation and type II hair cell regeneration
- Atoh1 overexpression enhances sustained recovery of vestibular function

Authors

Zahra N. Sayyid, Tian Wang, Leon Chen, Sherri M. Jones, Alan G. Cheng

Correspondence

aglcheng@stanford.edu

In Brief

The mature mouse utricle, which detects linear acceleration, displays limited regeneration, but whether function returns is unknown. Sayyid et al. show that regenerated hair cells appear and mature over months, resulting in a limited, unsustained functional recovery. Atoh1 overexpression enhances regeneration and leads to a sustained recovery of vestibular function.

Sayyid et al., 2019, Cell Reports *28*, 312–324
July 9, 2019
https://doi.org/10.1016/j.celrep.2019.06.028

CellPress

OPEN ACCESS
CellPress

Cell Reports
Report

Atoh1 Directs Regeneration and Functional Recovery of the Mature Mouse Vestibular System

Zahra N. Sayyid,[1] Tian Wang,[1] Leon Chen,[1] Sherri M. Jones,[2] and Alan G. Cheng[1,3,*]
[1]Department of Otolaryngology-Head and Neck Surgery, Stanford University School of Medicine, Stanford, CA 94305, USA
[2]Department of Special Education and Communication Disorders, College of Education and Human Sciences, University of Nebraska, Lincoln, NE 68583, USA
[3]Lead Contact
*Correspondence: aglcheng@stanford.edu
https://doi.org/10.1016/j.celrep.2019.06.028

SUMMARY

Utricular hair cells (HCs) are mechanoreceptors required for vestibular function. After damage, regeneration of mammalian utricular HCs is limited and regenerated HCs appear immature. Thus, loss of vestibular function is presumed irreversible. Here, we found partial HC replacement and functional recovery in the mature mouse utricle, both enhanced by overexpressing the transcription factor Atoh1. Following damage, long-term fate mapping revealed that support cells non-mitotically and modestly regenerated HCs displaying no or immature bundles. By contrast, Atoh1 overexpression stimulated proliferation and widespread regeneration of HCs exhibiting elongated bundles, patent mechanotransduction channels, and synaptic connections. Finally, although damage without Atoh1 overexpression failed to initiate or sustain a spontaneous functional recovery, Atoh1 overexpression significantly enhanced both the degree and percentage of animals exhibiting sustained functional recovery. Therefore, the mature, damaged utricle has an Atoh1-responsive regenerative program leading to functional recovery, underscoring the potential of a reprogramming approach to sensory regeneration.

INTRODUCTION

Sensory hair cells (HCs) are essential for vestibular function. In contrast to the cochleae, where no regeneration occurs (Bermingham-McDonogh and Reh, 2011), vestibular organs gradually replace lost HCs (Forge et al., 1993). The mammalian utricle, a vestibular organ that detects linear acceleration, displays new, immature HCs months after damage (Forge et al., 1993, 1998; Kawamoto et al., 2009). However, regeneration occurs almost exclusively in the peripheral zone termed the extrastriola, whereas the central striolar region fails to replace HCs (Golub et al., 2012). Many regenerated HCs bear short stereociliary bundles reminiscent of nascent, immature HCs (Forge et al., 1993; Kawamoto et al., 2009). Although vestibular HCs consist of two subtypes (types I and II), regenerated HCs have been reported to be almost exclusively type II (Bucks et al., 2017; Golub et al., 2012). Because regeneration is limited, loss of vestibular function is at present presumed irreversible.

Unlike the mammalian utricle, support cells in regenerating non-mammalian sensory organs mitotically regenerate both types of vestibular HCs to near complete levels throughout the organ (Roberson et al., 1992; Weisleder and Rubel, 1992), and function is restored as measured directly via vestibular physiology (Carey et al., 1996; Jones and Nelson, 1992). In mice, although behavior assessment using rotarod testing suggests some improvement of vestibular function months after injury (Schlecker et al., 2011), guinea pigs damaged by aminoglycosides failed to recover function as measured by vestibular evoked potential (VsEP) responses (Bremer et al., 2014). Therefore, it is unclear whether mammalian vestibular HC regeneration leads to restoration of function.

One proposed mechanism to enhance HC regeneration is via overexpression (OE) of Atoh1, a basic-helix-loop-helix transcription factor required for differentiation of developing HCs (Bermingham et al., 1999). In the developing cochlea and utricle, Atoh1 OE induced ectopic HC formation *in vivo* (Gao et al., 2016; Kelly et al., 2012; Liu et al., 2012). On the other hand, several studies have found limited to no ectopic HC formation after Atoh1 OE in the mature cochlea and utricle *in vivo*, indicating an age-related decline in Atoh1 responsiveness (Atkinson et al., 2014; Gao et al., 2016), which may be enhanced *in vitro* or after damage (Schlecker et al., 2011; Shou et al., 2003). In addition, HCs normally downregulate Atoh1 as they mature (Lanford et al., 2000), and constitutive Atoh1 OE in the cochlea prevents maturation (Liu et al., 2012). At present, it remains unclear whether transient or constitutive Atoh1 OE is effective in inducing HC regeneration and functional recovery in the mature mammal.

Here, we show that HCs regenerate and partially mature in the damaged, mature utricle, where Atoh1 OE stimulated proliferation of support cells and regeneration of HCs displaying elongated stereocilia and open mechanotransduction channels. Moreover, Atoh1 OE animals demonstrated more robust VsEP responses relative to damage-only animals. Thus, the damaged, mature mammalian utricle is uniquely competent to respond to Atoh1 OE to enhance both the number and maturation of regenerated HCs, resulting in improved vestibular function.

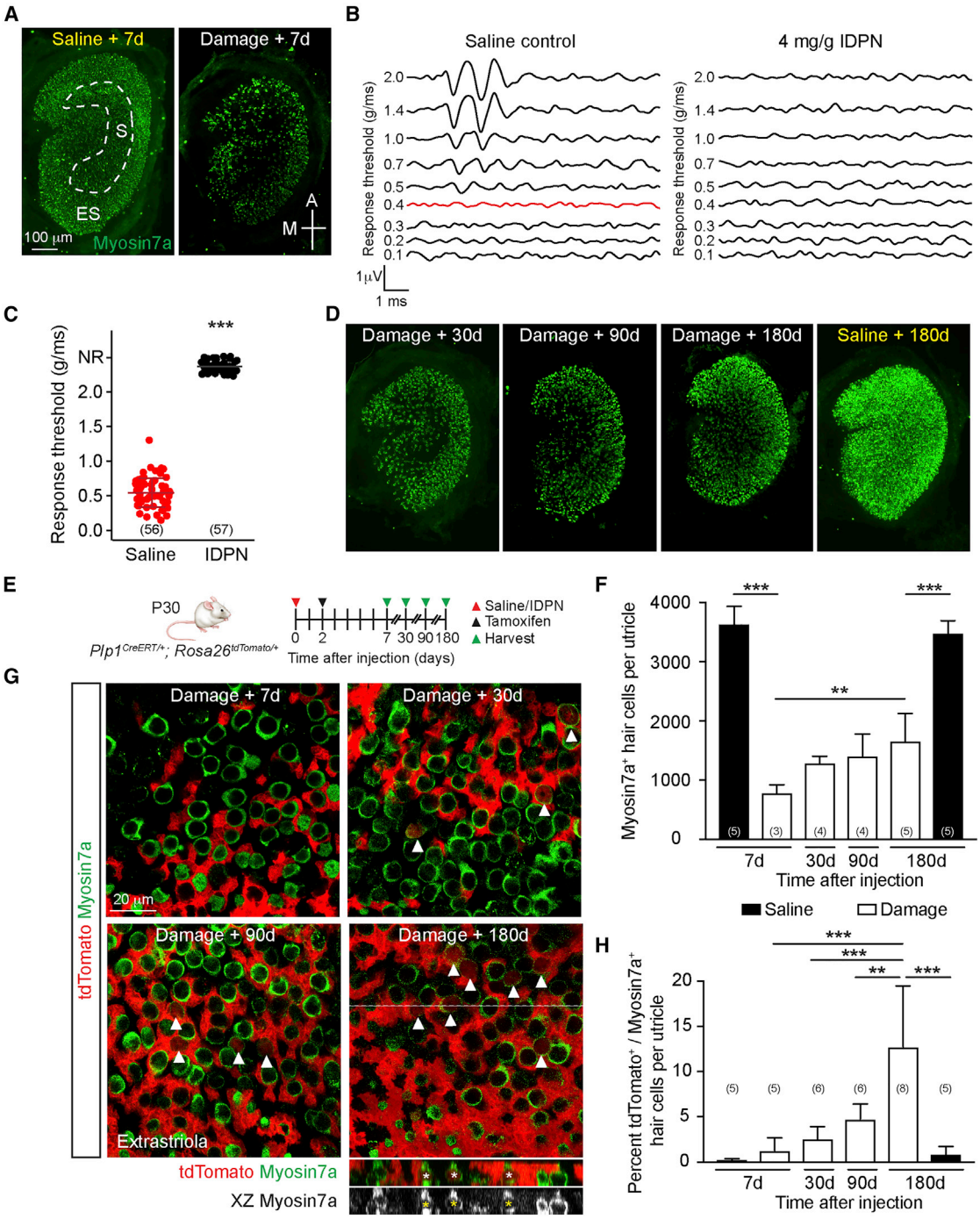

Figure 1. Plp1^{+} Support Cells Regenerate HCs

(A) P30 wild-type mice were treated with IDPN, and utricles were examined 1 week later. Undamaged controls were injected with saline. Myosin7a^{+} HCs were identified in the striola (dashed lines) and extrastriola.

(B) Characteristic VsEP waveforms from undamaged animals (threshold 0.4 g/ms, red) were lost in IDPN-treated animals.

(C) IDPN-treated animals displayed significantly higher thresholds than undamaged controls.

(D) Rapid loss followed by gradual repopulation of HCs.

(E) Schematic of transgenic approach to trace support cells.

(F) Quantification shows significant increase in total HC number in the entire organ by 180 days after damage.

(legend continued on next page)

RESULTS

HCs Spontaneously Regenerate in the Mature Mouse Utricle

We first developed and characterized a damage protocol using the vestibulotoxin IDPN (3,3′-iminodipropionitrile) (Soler-Martin et al., 2007). We administered IDPN to postnatal 30-day-old (P30) mice, an age when utricular function is deemed mature (Jones and Jones, 1999), and found that a moderate dose (4 mg/g) caused 68.2% and 76.3% HC loss in the extrastriola and striola, respectively, 7 days later (Figure 1A; Figures S1A–S1C).

VsEPs (vestibular evoked potentials) are compound action potentials elicited by linear acceleration in the naso-occipital axis (Jones et al., 2001, 2011). Threshold, latency, and amplitude of each waveform represent the overall organ sensitivity, timing of neural transmission, and size and synchrony of the activated neuronal population, respectively (Nazareth and Jones, 1998). Mutant mice with deficient stereociliary bundles or with HC loss demonstrate elevated thresholds, prolonged latencies, and decreased amplitudes (Geng et al., 2009; Krey et al., 2016), indicating that functional HCs are critical for VsEP responses. Seven days after IDPN treatment, animals demonstrated no detectable responses (Figure 1B). Overall, IDPN-treated animals showed significantly elevated thresholds, longer latencies, and smaller amplitudes compared with undamaged controls (Figure 1C; Figures S1D and S1E). Thus, IDPN treatment effectively decreased HC survival and abolished utricular function.

To assess for HC regeneration, we examined IDPN-treated animals with no detectable VsEP thresholds and found a gradual repopulation of HCs in the extrastriola but not the striola 30–180 days later (Figure 1D; Figure S1F), a finding consistent with other damage paradigms (Golub et al., 2012; Lin et al., 2011). Extrastriolar HC density increased from 29.3% of age-matched controls at 7 days to 56.8% at 180 days after damage (Table S1). Overall, total HC counts increased from 21.8% of age-matched controls at 7 days to 47.8% at 180 days (Figure 1F).

To label newly regenerated HCs, we traced support cells using *Plp1*$^{CreERT/+}$; *Rosa26*$^{tdTomato/+}$ mice (Plp1-Tomato; Figure 1E). After IDPN administration at P30 to ablate HCs, tamoxifen was given at P32 to activate Cre recombinase in support cells, labeling 75.0% of extrastriolar and 45.0% of striolar Sox2$^+$ support cells in both undamaged and damaged organs (Figures S2A and S2B). In the undamaged utricle, we found rare tdTomato$^+$, Myosin7a$^+$ HCs post-tamoxifen injection, corroborating previous reports of rare HC turnover (Figure S2C; Bucks et al., 2017). Seven days post-IDPN treatment, many traced support cells but no traced HCs were found. Mice injected with vehicle control without tamoxifen had minimal recombination (<1%) post-IDPN injection, indicating a low Cre recombinase leakiness as previously reported (Figure S2D; McGovern et al., 2017). After damage, traced HCs significantly increased in the extrastriola over time (Figures 1G and 1H; Figure S2E). In the striola, the increase in traced HCs was small, and the total number of HCs did not significantly increase over time (Figure S2E; Table S1). Together, these data indicate that support cells, particularly those in the extrastriola, contribute to HC regeneration in the mature, damaged mouse utricle.

Atoh1 Enhances HC Regeneration

During development, the transcription factor Atoh1 is essential for HC specification, and expression is downregulated postnatally (Bermingham et al., 1999; Lanford et al., 2000). In the undamaged mature utricle, HCs and support cells rarely express Atoh1 (fewer than two cells per 10,000 μm^2) (Figure S3A). Atoh1 was upregulated in support cells 7–14 days after IDPN treatment (Figures S3B and S3D). We postulated that incomplete, spontaneous regeneration is attributed to insufficient Atoh1 upregulation and hypothesized that Atoh1 OE could enhance HC regeneration. To test this, we used *Plp1*$^{CreERT/+}$; *CAG*$^{flox\text{-}Atoh1\text{-}HA/+}$ (henceforth Plp1-Atoh1-HA) mice (Liu et al., 2012), in which tamoxifen injection induces constitutive Atoh1 OE in support cells, which are in turn fate-mapped via the hemagglutinin (HA) tag (Figure 2A). Littermate controls sharing the same genetic background were used as damage-only controls.

Without damage, tamoxifen rarely induced Atoh1-HA expression and failed to stimulate ectopic HC formation (Figures S3E–S3H), despite robust Cre activation as detected by tdTomato expression (Figure S3I). In contrast, tamoxifen induced robust Atoh1-HA expression in support cells in the damaged utricle (Figure S4A; Table S2). Moreover, significantly more regenerated HCs were observed over time, reaching 80.4% of undamaged, age-matched controls 180 days post-damage (Figures 2B and 2C). Although HCs regenerated mainly in the extrastriola of damage-only utricles (Figures 2D and 2E; Table S1), Atoh1 OE, damaged utricles showed significantly more HCs in both the extrastriola and striola (Figures 2D–2F; Table S1), resulting in significantly more HCs overall.

Atoh1 OE, damaged utricles showed a gradual and significant increase in traced, HA$^+$ HCs over time (Figures 2D–2F; Tables S1 and S2), suggesting that Atoh1 OE increased support cell conversion into HCs only after damage. In support of this notion, Atoh1 OE significantly increased Atoh1$^+$ support cells only after damage (Figures S3B–S3D). Together, these results suggest that support cells in the damaged, mature utricle are competent to respond to Atoh1 OE and regenerate more HCs.

Atoh1 OE Increases Proliferation

The mature mammalian utricle is mitotically quiescent and remains so after damage. To assess for proliferation early (1 week) and late (1–3 months) post-damage, we immunostained for Ki67 or injected EdU intraperitoneally 3 days per week for 4 weeks. We detected almost no labeled support cells in either damage-only or Atoh1 OE undamaged utricles (Figures 2G–2I; Table S3). By contrast, Atoh1 OE, damaged utricles had Ki67$^+$/Sox2$^+$ (4.4 ± 9.6 per utricle, n = 10) and

(G) Traced HCs increase post-IDPN treatment (arrowheads). Orthogonal projection showing traced HCs (asterisks) 180 days post-damage.
(H) Quantification of traced HCs.
Student's t test (C), one-way ANOVA with Tukey's multiple comparisons test (F and H), n for animals (C) and utricles (F and H). **p < 0.01, ***p < 0.001. Data are shown as mean ± SD.

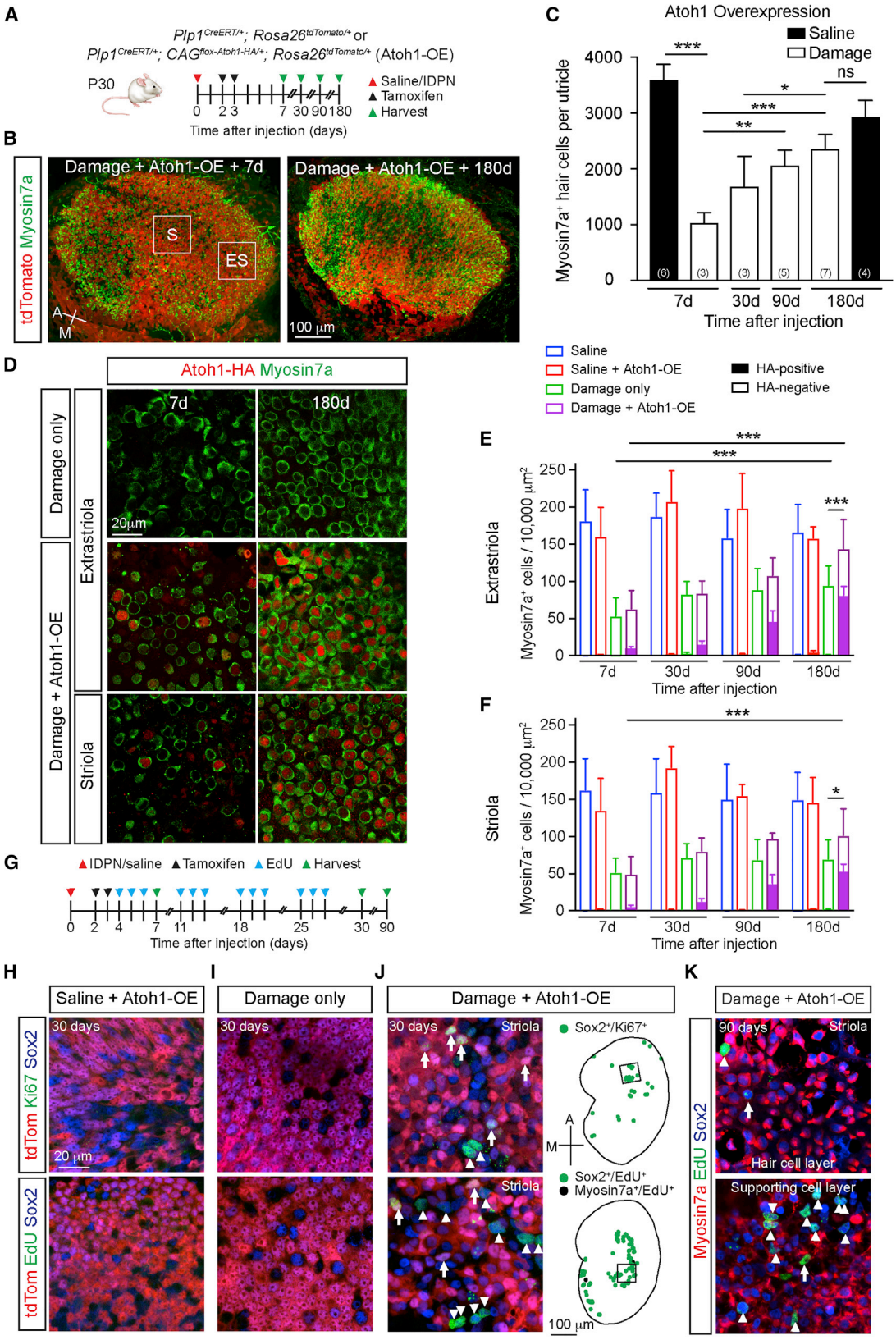

(legend on next page)

$EdU^+/Sox2^+$ (20.9 ± 37.3, n = 19) support cells primarily in the striola 30 days post-damage (Figure 2J; Figure S4B). Overall, among the 19 utricles analyzed 30 days post-damage and Atoh1 OE, 7 showed proliferating cells, with a small subset of EdU^+ cells expressing Myosin7a (Figure 2J). Significantly more $EdU^+/Sox2^+$ support cells were found in Atoh1 OE, damaged utricles than in damage-only utricles (0.0 ± 0.0, n = 3, $p < 0.05$). Most EdU^+ cells were not tdTomato or HA labeled (Figure 2J; Figures S4B and S4C), suggesting that Atoh1 may have stimulated proliferation in a non-cell-autonomous manner. Ninety days after damage and Atoh1 OE, many $EdU^+/Sox2^+$ but no $Ki67^+/Sox2^+$ cells were found (Figure 2K), suggesting that mitotic cells did not degenerate and mitosis was transient. These data demonstrate that Atoh1 OE induces support cell proliferation of the damaged mouse utricle.

Atoh1 Enhances Stereociliary Bundle Formation

HCs are equipped with stereociliary bundles that lengthen as they mature (Geleoc and Holt, 2003). Months after injury, the mammalian utricle contains HCs bearing short bundles reminiscent of nascent HCs (Forge et al., 1993). We sought to assess the bundles, a presumed surrogate marker of maturation (Ellwanger et al., 2018), of regenerated HCs by labeling for F-actin post-damage (Figure 3A). The apical surface of undamaged utricles is composed of a sheet of HCs with dense, mature stereociliary bundles (Figure 3B). In contrast, 7 days post-damage, most bundles have disappeared, as >77% of HCs are lost (Figures S5A and S5B). At 30 days, 69.8% of traced, regenerated HCs lacked bundles (i.e., bundleless), while 30.2% displayed a spectrum of bundle maturity, most of which appeared short (Figures 3C, 3F, S5C, and S5D). In contrast, bundles were detected on more traced HCs 90–180 days post-damage (Figures 3C and 3F). In comparison, 83.4% of untraced HCs, which represent surviving HCs and some newly regenerated but untraced HCs, displayed bundles 30 days after damage (Figure 3G). By 180 days, 96.4% of untraced HCs displayed bundles (Figures 3B and 3G). Thus, our data suggest that the apical maturation of regenerated HCs was incomplete, even after a prolonged recovery post-injury.

Constitutive Atoh1 OE restricts HC maturation in the cochlea, resulting in a lack of terminal differentiation markers and bundle development (Atkinson et al., 2014). To determine whether Atoh1 OE regenerated HCs in the utricle can mature, we first examined Atoh1 OE, undamaged tissues and found no bundle abnormalities (Figure 3D). When examining Atoh1 OE, damaged tissues at 30 days, we found that like damage-only tissues, >50% of traced, regenerated HCs were bundleless (Figures 3E and 3F). Unexpectedly, significantly more Atoh1 OE traced HCs displayed bundles 90 (94.0%) and 180 days (95.5%) post-damage compared with damage-only HCs (Figures 3E and 3F).

To assess for functionality of regenerated HCs, we applied Texas red-tagged gentamicin (GTTR), which selectively permeates mechanotransduction channels (Alharazneh et al., 2011). In Atoh1 OE, undamaged utricles, 83.8% of HCs were $GTTR^+$, and no HA^+ HCs were detected (Figures 3H and 3J). In contrast, numerous HA^+ HCs were present throughout the Atoh1 OE, damaged utricle (Figure 3I), in which 64.6% of $Myosin7a^+/HA^-$ HCs and 32.6% of $Myosin7a^+/HA^+$ incorporated GTTR (Figures 3I and 3J). Taken together, these data suggest that Atoh1 OE regenerated HCs matured and gained the ability to take up GTTR, indicative of patent mechanotransduction channels. Moreover, Atoh1 OE promotes the development of mature-appearing bundles in regenerated HCs.

Regenerated HCs Differentiate into HC Subtypes

The mature mouse utricle is composed of two main subtypes of HCs, estimated to be 55% type I and 45% type II (Desai et al., 2005). Type I HCs express osteopontin (OPN) at the apical neck and are innervated by flask-shaped calyces, whereas type II HCs express a membranous pattern of annexin A4 (ANXA4) and are innervated by boutons (Figure 4C; McInturff et al., 2018). We found that progressively more traced HCs expressed OPN and fewer expressed ANXA4 after damage (Figures 4A, 4D, 4E, 4H, and 4I). By 180 days post-damage, with traced regenerated HCs significantly increased, the proportion of OPN^+ traced HCs increased, whereas that of $ANXA4^+$ traced HCs decreased (Figures 4A, 4D, 4E, 4H, and 4I), suggesting that more HCs with a type I phenotype regenerated over time. In support of this notion, traced HCs associated with $Tuj1^+$ calyces increased from 5.5% at 30 days to 12.9% 180 days after damage (Figure 4J; Figure S6A). Altogether, our data suggest that regenerated HCs consist of both type I and type II HCs.

Figure 2. Atoh1 OE Enhances HC Regeneration and Proliferation

(A) Schematic for tracing and Atoh1 OE in $Plp1^+$ support cells. Atoh1 OE cells were detected via tdTomato/HA labeling.

(B) Robust repopulation of Atoh1 OE, damaged utricles with $tdTomato^+$ HCs. Boxes represent extrastriolar and striolar regions where high-magnification images were taken.

(C) Quantification of total HCs post-treatment (IDPN or saline) and Atoh1 OE.

(D) Representative images of the extrastriola and striola after damage alone or with Atoh1 OE. No HA^+ cells were identified after damage alone. HA^+ HCs were detected after damage and Atoh1 OE.

(E and F) Extrastriolar (E) and striolar (F) HC density in undamaged, damaged only, Atoh1 OE, undamaged, and Atoh1 OE, damaged tissues.

(G) Schematic to ablate HCs, fate-map $Plp1^+$ support cells, and Atoh1 OE. EdU was given to label mitotic cells.

(H and I) No $Ki67^+$ or EdU^+ cells were detected in the sensory epithelium of either Atoh1 OE, undamaged (H) or damage-only (I) utricles at 30 days.

(J) $Ki67^+$ and EdU^+ support cells were detected 30 days after damage and Atoh1 OE, particularly in the striola. tdTomato-positive (arrow) and tdTomato-negative (arrowheads) proliferative ($Ki67^+$ or EdU^+) cells. Drawings depicting location of proliferative $Sox2^+$ (green) and $Myosin7a^+$ (black) cells; black boxes represent striolar regions where images were captured.

(K) Ninety days after damage and Atoh1 OE, many EdU^+ cells were still detected in the striola, consisting of $EdU^+/Sox2^+/Myosin7a^-$ support cells (arrowheads) and $EdU^+/Sox2^+/Myosin7a^+$ HCs (arrows).

One-way ANOVA with Tukey's multiple comparisons test (C), two-way ANOVA with Tukey's multiple comparisons test (E and F), n for utricles. *$p < 0.05$; **$p < 0.01$, ***$p < 0.001$. Data are shown as mean ± SD.

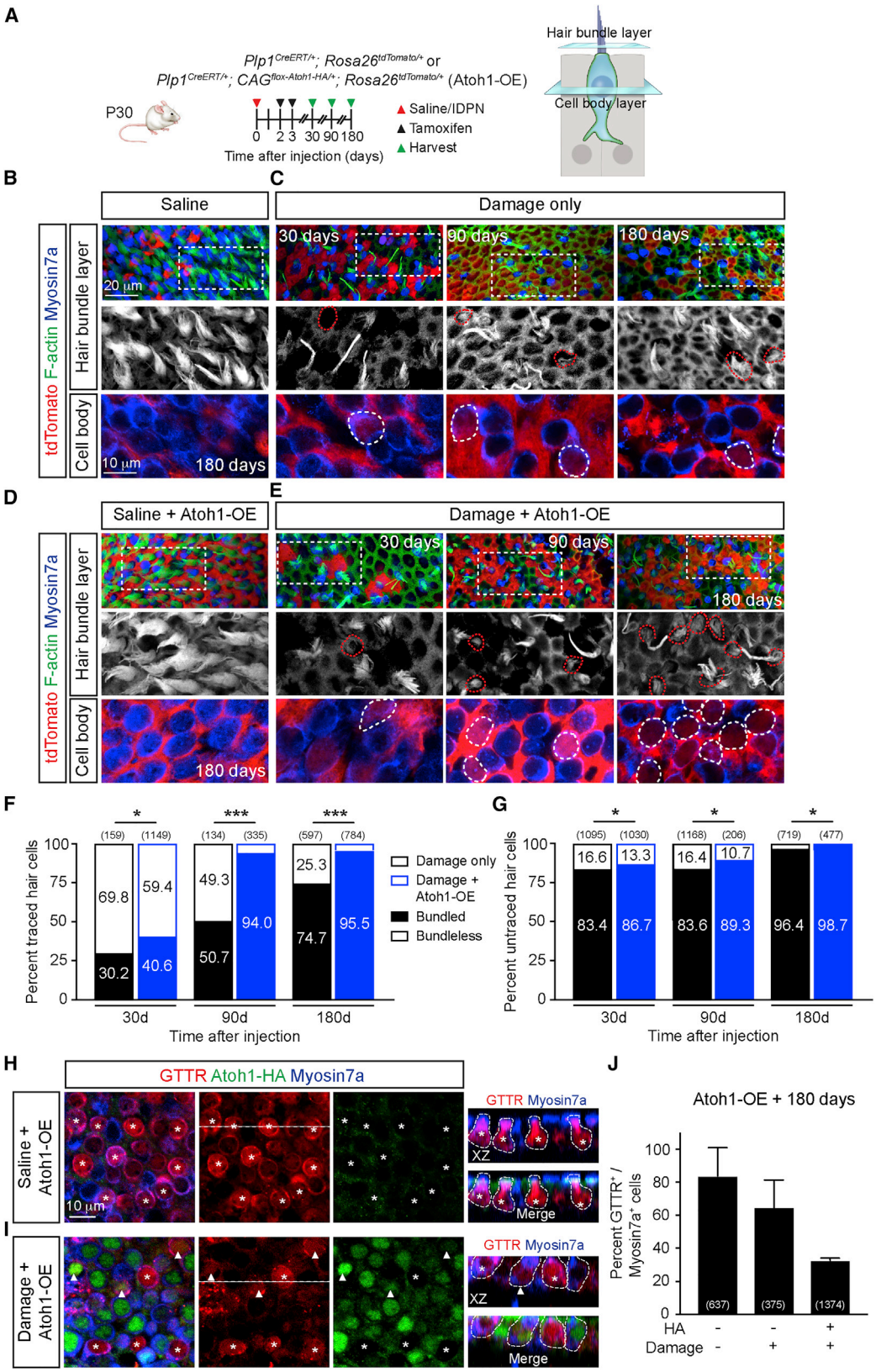

(legend on next page)

In the Atoh1 OE, damaged utricle, traced HCs predominantly (>93%) expressed the type II HC marker ANXA4 across all time points examined (Figures 4B, 4G, and 4I). Despite an increase in regenerated HCs as a result of Atoh1 OE, the proportion of OPN$^+$ traced HCs remained low (Figures 4B, 4F, and 4H). Moreover, traced HCs rarely displayed Tuj1$^+$ calyces (Figure 4J). As controls, untraced HCs from damage-only and Atoh1 OE, damaged utricles showed a similar percentage of OPN, ANXA4, and Tuj1 expression across time points (Figures S6B–S6E). All traced, regenerated HCs in both damage-only and Atoh1 OE, damaged utricles were juxtaposed to Tuj1$^+$ neurites and appeared innervated. They also had comparable expression of the pre- and post-synaptic markers Ctbp2 and Shank1, respectively (Figure S6F). These data suggest that Atoh1 OE regenerated HCs acquired a type II HC phenotype at the expense of type I HCs, displayed synaptic elements and appeared innervated.

Atoh1 OE Improves Recovery of Vestibular Function

The avian utricle can regenerate both type I and type II HCs to regain VsEP responses (Jones and Nelson, 1992). We sought to determine whether spontaneous regeneration—in which we have observed a modest regeneration of both type I and type II HCs—or Atoh1-enhanced regeneration—in which we observed type II HC phenotypes, elongated stereociliary bundles, and neural integration—leads to a recovery of vestibular function of the damaged, mature mouse utricle. After initial loss of vestibular function at 7 days, VsEP responses were measured 30, 90, and 180 days after IDPN treatment (Figure 5A). Undamaged, control animals displayed consistent VsEP thresholds at all time points, and Atoh1 OE did not affect thresholds in the undamaged control (Figures 5B and 5C). Many IDPN-treated animals continued to have no measurable response 30 days after damage but regained a partial recovery of responses by 180 days (Figure 5B). These responses, however, remained abnormal as thresholds were higher, latencies longer, and amplitudes smaller than those of age-matched controls (Figures 5B and 5C; Figures S7B and S7C).

Average VsEP thresholds significantly improved from 7–180 days after IDPN treatment but remained significantly higher than undamaged control levels (Figure 5C). After an initial improvement 30–90 days post-damage, average thresholds of damage-only animals worsened at 180 days, suggesting that improvement in responses may be temporary and unsustained over time. In comparison, average thresholds of Atoh1 OE, damaged animals were significantly better than damage-only animals at 180 days (Figure 5C). Additionally, significantly more Atoh1 OE, damaged animals displayed VsEP responses at 180 days than damage-only animals (Figure 5D).

Both latencies and amplitudes significantly improved over time but remained significantly worse than age-matched controls in both damage-only and Atoh1 OE, damaged animals at 180 days (Figures S7B–S7D), suggesting that the timing of neural transmission was prolonged, and resynchronization of vestibular ganglia firing remained incomplete. Latencies and amplitudes did not significantly differ between damage-only and Atoh1 OE, damaged animals (Figure S7D), suggesting that neural connections of Atoh1 OE regenerated HCs were comparable with those of regenerated HCs in damage-only organs. In support of these results, we detected no gross differences in synaptic protein (Ctbp2 and Shank1) expression in HCs from the two groups (Figure S6F). When comparing HC densities in utricles from individual damaged animals to their corresponding VsEP thresholds, we found a significant correlation (Figures 5E and 5F), suggesting that HC regeneration may have contributed to the functional recovery.

To follow the vestibular function of individual animals over time, we serially measured VsEPs in a subset of animals 7–180 days post-treatment (11 control and 29 damaged for spontaneous regeneration, 5 control and 19 damaged for Atoh1-enhanced regeneration). As expected, all control animals displayed stable thresholds (Figures 5G and 5H). After an initial loss of thresholds in damaged-only animals, we found three trajectories for vestibular function: (1) no recovery (17.2%), (2) sustained recovery (37.9%), and (3) unsustained recovery (44.8%) as defined by an initial recovery of thresholds followed by a subsequent loss by 180 days (Figure 5G; Table S4). Although >50% of serially analyzed mice recovered VsEP thresholds at 30 and 90 days, <40% of mice had detectable thresholds by 180 days (Figures 5D and 5G). Together, these data suggest that during spontaneous regeneration, 82.8% of animals (24 of 29) are able to partially recover vestibular function, but 54.2% of these animals (13 of 24) failed to recover function in a sustained manner. Among the 19 Atoh1 OE, damaged mice, 21.1% demonstrated no recovery, 68.4% sustained recovery, and 10.5% unsustained recovery (Figure 5H; Table S4). In comparison with damage-only animals,

Figure 3. Atoh1 OE Enhances Stereociliary Bundle Formation

(A) Schematic showing the strategy for ablating HCs, tracing and Atoh1 OE in Plp1$^+$ support cells. *Plp1*$^{CreERT/+}$; *Rosa26*$^{tdTomato/+}$ mice served as controls.

(B) Undamaged utricles contained many HCs with healthy and long bundles and no traced HCs. Dashed boxes represent areas from which high-magnification images at the hair bundle and cell body levels are shown.

(C) Thirty days after damage, many HCs were lost, and the few traced HCs (dashed lines) present displayed no stereociliary bundles. Ninety and 180 days after damage, more traced HCs appeared, many displaying stereociliary bundles.

(D) Atoh1 OE, undamaged control utricle show normal HC density and bundle morphology.

(E) With damage and Atoh1 OE, many more traced HCs (dashed lines) gradually appeared, most noticeably at 90 and 180 days. Bundles were detected in most traced HCs.

(F and G) Percentage of traced (F) and untraced (G) HCs in damage-only and Atoh1 OE, damaged utricles displaying stereociliary bundles months after damage.

(H and I) Representative images of Atoh1 OE, undamaged (H) and damaged (I) utricles at 180 days. Utricles were incubated with GTTR. In undamaged tissues, all HCs were negative for HA, and most were GTTR$^+$ (asterisks). With damage and Atoh1 OE, GTTR labeling was observed in Myosin7a$^+$/HA$^+$ (arrowheads) and Myosin7a$^+$/HA$^-$ HCs (asterisks).

(J) Quantification of Myosin7a$^+$/GTTR$^+$ HCs in Atoh1 OE, undamaged and damaged utricles at 180 days.

χ^2 test, n for HCs. *p < 0.05; **p < 0.01, ***p < 0.001. Data are shown as mean ± SD.

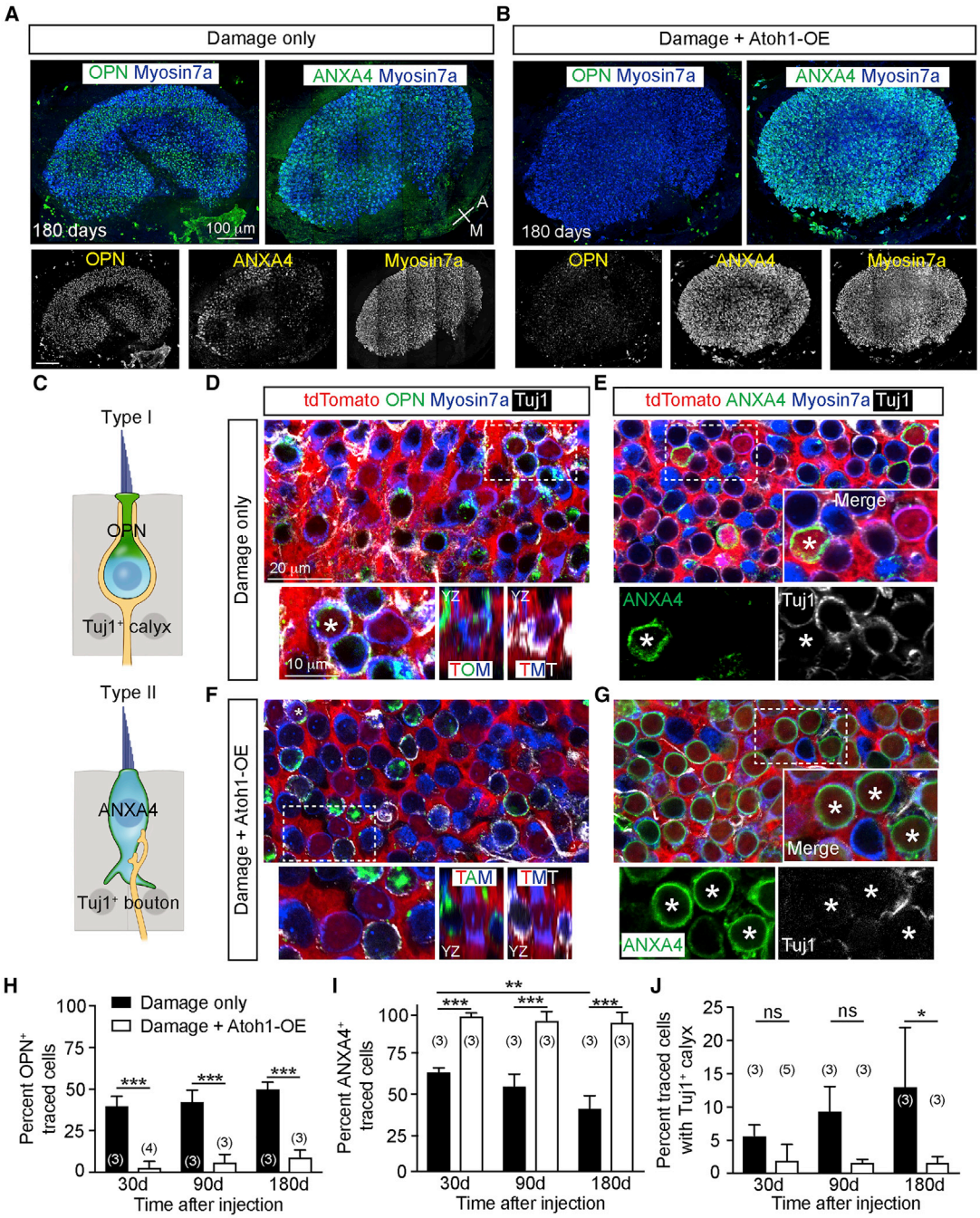

Figure 4. Atoh1 OE Increases Regeneration of Neurally Integrated Type II HCs

(A and B) Damaged-only (A) and Atoh1 OE, damaged (B) utricles demonstrating osteopontin$^+$ (OPN) type I HCs and annexin A4$^+$ (ANXA4) type II HCs. After damage and Atoh1 OE, the utricle was densely populated by HCs, with a noticeable loss of OPN expression.

(C) Diagram depicting amphora-shaped type I HCs expressing OPN in the neck region and goblet-shaped type II HCs expressing membranous ANXA4.

(D) Representative images of damaged utricles at 180 days showing traced, Myosin7a$^+$, OPN$^+$ type I HCs (asterisk) with Tuj1$^+$ calyx (orthogonal view highlighting OPN and Tuj1 labeling). Traced HCs negative for OPN were also noted.

(E) Many traced Myosin7a$^+$, ANXA4$^+$ type II HCs (asterisk) without Tuj1$^+$ calyces were found, alongside traced HCs negative for ANXA4.

(F) After damage and Atoh1 OE, there was a noticeable loss of OPN expression and Tuj1$^+$ calyces among traced Myosin7a$^+$ HCs (orthogonal view illustrating loss of OPN labeling). A rare traced Myosin7a$^+$, OPN$^+$ type I HC (asterisk) identified with a Tuj1$^+$ calyx.

(G) Most traced Myosin7a$^+$ HCs expressed ANXA4 without Tuj1$^+$ calyces. High-magnification images showing traced HCs expressing ANXA4$^+$ (asterisks).

(H–J) Quantification of traced HCs expressing OPN (H), ANXA4 (I), and displaying calyces (J).

Two-way ANOVA with Tukey's multiple comparisons test, n for utricles. *$p < 0.05$; **$p < 0.01$, ***$p < 0.001$. Data are shown as mean ± SD.

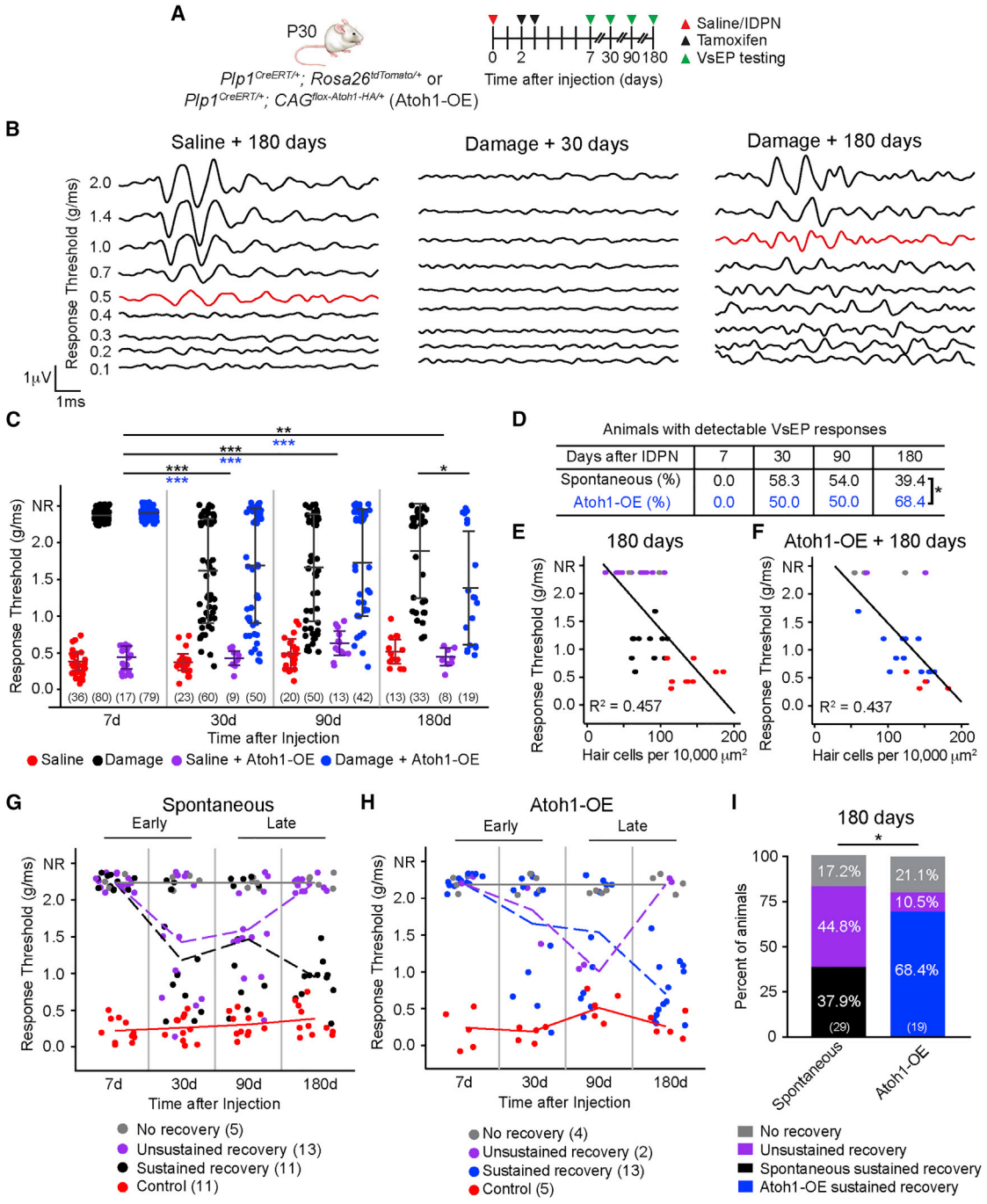

Figure 5. Atoh1 OE Enhances Functional Recovery of the Damaged, Mature Utricle

(A) Schematic showing experiments measuring VsEPs in control and damaged mice with and without Atoh1 OE.

(B) Representative VsEP traces of control animals 180 days after saline treatment (threshold 0.5 g/ms, red) and animals 30 (no responses) and 180 days after IDPN treatment (threshold 1.0 g/ms, red).

(C) VsEP thresholds of saline-treated (red), damage-only (black), Atoh1 OE, saline-treated (purple), and Atoh1 OE, damaged (blue) animals.

(D) Percentage of animals with detectable VsEP responses.

(E and F) Significant correlation between VsEP thresholds of damage-only (E) and Atoh1 OE, damaged (F) animals and utricular HC density at 180 days post-treatment.

(G) Serial measurements of individual animals show three patterns: no recovery (gray), unsustained recovery (purple), and sustained recovery (black). Control animals in red.

(legend continued on next page)

significantly more animals showed a sustained recovery of VsEP responses (Figure 5I). In sum, the mature mouse utricle can partially regain function following damage, but the recovery is commonly unsustained. In contrast, Atoh1 OE leads to a sustained recovery of vestibular function.

DISCUSSION

The mature mammalian cochlea fails to regenerate lost HCs, leading to permanent hearing loss. Although HCs regenerate in the mature mammalian vestibular organs (Forge et al., 1993; Golub et al., 2012; Li et al., 1995; Warchol et al., 1993), whether this limited degree of regeneration leads to a recovery of vestibular function was previously unknown. Here, we demonstrate that the mature mouse utricle is capable of spontaneous and modest regeneration of HCs and recovery of vestibular function over a 6 month time course. Moreover, functional recovery was in part unsustained, leading to a detectable VsEP response in <40% of animals 180 days post-damage. Atoh1 OE significantly increased HC regeneration throughout the utricle, stimulated proliferation, and promoted bundle formation. Overall, Atoh1 OE improved VsEP responses leading to sustained functional recovery in more animals (Figure S8). Collectively, we have revealed that Atoh1 OE promotes vestibular regeneration and functional recovery.

Incomplete Bundle Maturation in Regenerated HCs

We found that regenerating HCs displayed nascent or no bundles, starkly contrasting their more mature basolateral features (HC subtype markers, synaptic proteins, and nerve terminals). In the developing utricle, specified HCs first acquire bundles and mechanotransduction and subsequently basolateral potassium currents and nerve terminals characteristic of HC subtype specialization (Geleoc et al., 2004). Therefore, unlike developing HCs, apical bundles in regenerating HCs fail to mature despite grossly normal synaptic elements and innervation (Atkinson et al., 2015; Zheng and Zuo, 2017; Wang et al., 2019). Such discrepancies in the degrees of maturation of bundles and basolateral features were previously observed in ectopic HCs in the neonatal and mature cochlea and HCs derived from embryonic stem cells (Gubbels et al., 2008; Oshima et al., 2010; Walters et al., 2017).

Damage-Induced Atoh1 Responsiveness

Atoh1 induces ectopic HC formation in the immature cochlea and utricle (Gao et al., 2016; Kelly et al., 2012; Liu et al., 2012). However, the efficacy of Atoh1 in the mature inner ear is rather limited, as the few Atoh1 OE HCs failed to mature (Atkinson et al., 2014; Liu et al., 2012). After damage, the mature cochlea remains minimally responsive to Atoh1 (Atkinson et al., 2014; Liu et al., 2012). Our results indicate that the damaged mature utricle, but not the undamaged organ, is competent to respond to Atoh1 OE.

Atoh1-HA was rarely detected in the undamaged utricle, but HA-negative cells could be expressing HA at low levels, as HA immunostaining is less sensitive than tdTomato expression. Higher Atoh1-HA levels in the Atoh1 OE, damaged organs may have increased regeneration by enhancing endogenous Atoh1 levels, as the two can correlate at transcription levels during regeneration (Yamashita et al., 2018). Further investigation examining transcription factor networks in the damaged mature utricle can help identify mechanisms of Atoh1 responsiveness.

Multiple Effects of Atoh1 OE on Vestibular Regeneration

Constitutive expression of Atoh1 stimulates ectopic HC formation, yet new HCs fail to fully mature, presumably because of a lack of Atoh1 downregulation (Liu et al., 2012; Yamashita et al., 2018). Our data suggest that sustained Atoh1 OE enhances, rather than prevents, apical maturation of regenerating HCs. Forced expression of Atoh1 was previously reported to induce bundle repair in noise-damaged cochlear HCs (Yang et al., 2012), lending additional evidence that Atoh1 OE can promote bundle formation.

Atoh1 OE also stimulated support cell proliferation, a response previously noted in the neonatal mouse and avian cochlea (Kelly et al., 2012; Lewis et al., 2012). Proliferative cells primarily occupied the striola, suggesting regional differences in proliferative capacity. Previous work on the neonatal mouse utricle showed that damage induced cell cycle re-entry in $Lgr5^{+}$ striolar support cells (Wang et al., 2015). Because most proliferative cells were not traced, Atoh1 OE may have stimulated mitosis in a non-cell-autonomous manner while promoting HC specification and maturation in a cell-autonomous fashion. Comparing Atoh1 target genes in vestibular and cochlear tissues (Yamashita et al., 2018) should shed light on possible mechanisms differentiating their responsiveness.

The degree of HC regeneration induced by Atoh1 OE exceeds that of spontaneous regeneration, although it remained incomplete relative to undamaged tissues. Because our transgenic approach constitutively introduced a single, extra copy of Atoh1, it is possible that other strategies to overexpressing Atoh1 (e.g., transient and/or multiple copies of Atoh1) may induce different effects.

Vestibular Regeneration and Function

VsEP responses are thought to originate largely from the activation of type I HCs because of their larger conductances (Kim et al., 2011). However, during avian vestibular regeneration, responses return within 7–14 days after damage, when predominantly type II HCs with nascent stereociliary bundles repopulate the epithelium and before type I HCs emerge (Dye et al., 1999; Jones and Nelson, 1992; Weisleder et al., 1990). In our study, Atoh1 OE enhanced regeneration of predominantly type II HCs, leading to improved, sustained functional recovery. This suggests that utricles containing mainly type II HCs may also

(H) Serial measurements of individual animals show three patterns: no recovery (gray), unsustained recovery (purple), and sustained recovery (blue). Control animals in red.

(I) Percentage of animals in each recovery group at 180 days after IDPN treatment.

Two-way ANOVA with Tukey's multiple-comparisons test (C), χ^2 test (D and I), linear regression for Pearson correlation coefficient (E and F), n for animals. *p < 0.05; **p < 0.01, ***p < 0.001. Data are shown as mean ± SD.

function to detect linear acceleration and contribute to VsEP responses. In both spontaneous and Atoh1-enhanced regeneration, HC number correlated with vestibular responses. However, we did not observe a threshold of HC number above which vestibular function more readily recovers.

In the late phase of recovery of vestibular function, we propose that unsustained recovery may have resulted from dysfunction and subsequent loss of regenerated HCs. Regenerating HCs may be susceptible to delayed degeneration, a phenomenon previously observed in the regenerating neonatal cochlea (Atkinson et al., 2018; Cox et al., 2014). Alternatively, insufficient levels of Atoh1 may have caused unsustained recovery during regeneration, and Atoh1 OE may have promoted the maturation and survival of regenerated HCs, which in turn converted animals with unsustained recovery to a sustained recovery pattern. Moreover, the recovery of surviving HCs, striolar HC regeneration and support cell proliferation as a result of Atoh1 OE may have also contributed to improved vestibular function. Other potential contributing factors to the recovery of vestibular function include changes in innervation and synapse formation. In addition to causing HC damage, IDPN is also a neurotoxin targeting neurons in the central and peripheral vestibular systems (Llorens et al., 2011), possibly causing some variability of VsEP results. Our current model is ideal to further investigate the significance of each component in future works.

Our study posits Atoh1 as a promising candidate target to induce regeneration of vestibular sensory organs to restore function. As bona fide HC progenitors, support cells in the damaged mature utricle may reveal factors conferring Atoh1 responsiveness, which should guide future reprogramming approaches for inner ear regeneration.

STAR★METHODS

Detailed methods are provided in the online version of this paper and include the following:

- KEY RESOURCES TABLE
- LEAD CONTACT AND MATERIALS AVAILABILITY
- EXPERIMENTAL MODEL AND SUBJECT DETAILS
  - Mice
- METHOD DETAILS
  - Genotyping
  - Vestibular physiology
  - Immunohistochemistry
- QUANTIFICATION AND STATISTICAL ANALYSIS
  - Image acquisition and cell quantification
  - Statistical analyses

SUPPLEMENTAL INFORMATION

Supplemental Information can be found online at https://doi.org/10.1016/j.celrep.2019.06.028.

ACKNOWLEDGMENTS

We thank our lab members, R. Nusse, S. Heller, and J. Raymond for fruitful discussion, W. Dong, M. O'Sullivan, N. Grillet, D. Hosseini, Y. Ma, S. Vijayakumar, K. Hotovy, and M. Rosdail for excellent technical support, C. Gralapp for illustration, and J. Zuo for mouse sharing. This work was supported by the Stanford Medical Scholars Research Program, Howard Hughes Medical Institute Medical Fellows Program, Stanford MSTP, and NIH/National Institute on Deafness and Other Communication Disorders (NIDCD) grant F30DC015698 (Z.N.S.); the Lucile Packard Foundation for Children's Health and Stanford NIH/National Center for Advancing Translational Sciences (NCATS) Clinical and Translational Science Award (CTSA) UL1 TR001085; the Child Health Research Institute of Stanford University and NIH/NIDCD grant R21DC015879 (T.W.); Nebraska Tobacco Settlement Biomedical Research Development Funds (S.M.J.); and NIH/NIDCD grants K08DC011043, RO1DC013910, and RO1DC016919, Department of Defense grant MR130316, the Akiko Yamazaki and Jerry Yang Faculty Scholar Fund, and California Institute for Regenerative Medicine grants RN3-06529 and DISC2-10537 (A.G.C.).

AUTHOR CONTRIBUTIONS

Z.N.S., T.W., S.M.J., and A.G.C. designed experiments. Z.N.S., L.C., T.W., S.M.J., and A.G.C. performed experiments and analyzed data. Z.N.S., T.W., S.M.J., and A.G.C. wrote the manuscript.

DECLARATION OF INTERESTS

A.G.C. is a scientific advisor for Decibel Therapeutics.

Received: November 1, 2018
Revised: February 13, 2019
Accepted: June 6, 2019
Published: July 9, 2019

REFERENCES

Alharazneh, A., Luk, L., Huth, M., Monfared, A., Steyger, P.S., Cheng, A.G., and Ricci, A.J. (2011). Functional hair cell mechanotransducer channels are required for aminoglycoside ototoxicity. PLoS ONE *6*, e22347.

Atkinson, P.J., Wise, A.K., Flynn, B.O., Nayagam, B.A., and Richardson, R.T. (2014). Hair cell regeneration after ATOH1 gene therapy in the cochlea of profoundly deaf adult guinea pigs. PLoS ONE *9*, e102077.

Atkinson, P.J., Huarcaya Najarro, E., Sayyid, Z.N., and Cheng, A.G. (2015). Sensory hair cell development and regeneration: similarities and differences. Development *142*, 1561–1571.

Atkinson, P.J., Dong, Y., Gu, S., Liu, W., Najarro, E.H., Udagawa, T., and Cheng, A.G. (2018). Sox2 haploinsufficiency primes regeneration and Wnt responsiveness in the mouse cochlea. J. Clin. Invest. *128*, 1641–1656.

Bermingham, N.A., Hassan, B.A., Price, S.D., Vollrath, M.A., Ben-Arie, N., Eatock, R.A., Bellen, H.J., Lysakowski, A., and Zoghbi, H.Y. (1999). Math1: an essential gene for the generation of inner ear hair cells. Science *284*, 1837–1841.

Bermingham-McDonogh, O., and Reh, T.A. (2011). Regulated reprogramming in the regeneration of sensory receptor cells. Neuron *71*, 389–405.

Bremer, H.G., Versnel, H., Hendriksen, F.G., Topsakal, V., Grolman, W., and Klis, S.F. (2014). Does vestibular end-organ function recover after gentamicin-induced trauma in Guinea pigs? Audiol. Neurotol. *19*, 135–150.

Bucks, S.A., Cox, B.C., Vlosich, B.A., Manning, J.P., Nguyen, T.B., and Stone, J.S. (2017). Supporting cells remove and replace sensory receptor hair cells in a balance organ of adult mice. eLife *6*, e18128.

Carey, J.P., Fuchs, A.F., and Rubel, E.W. (1996). Hair cell regeneration and recovery of the vestibuloocular reflex in the avian vestibular system. J. Neurophysiol. *76*, 3301–3312.

Cox, B.C., Chai, R., Lenoir, A., Liu, Z., Zhang, L., Nguyen, D.H., Chalasani, K., Steigelman, K.A., Fang, J., Cheng, A.G., et al. (2014). Spontaneous hair cell regeneration in the neonatal mouse cochlea in vivo. Development *141*, 816–829.

Desai, S.S., Zeh, C., and Lysakowski, A. (2005). Comparative morphology of rodent vestibular periphery. I. Saccular and utricular maculae. J. Neurophysiol. *93*, 251–266.

Doerflinger, N.H., Macklin, W.B., and Popko, B. (2003). Inducible site-specific recombination in myelinating cells. Genesis *35*, 63–72.

Dye, B.J., Frank, T.C., Newlands, S.D., and Dickman, J.D. (1999). Distribution and time course of hair cell regeneration in the pigeon utricle. Hear. Res. *133*, 17–26.

Ellwanger, D.C., Scheibinger, M., Dumont, R.A., Barr-Gillespie, P.G., and Heller, S. (2018). Transcriptional dynamics of hair-bundle morphogenesis revealed with CellTrails. Cell Rep. *23*, 2901–2914.e13.

Forge, A., Li, L., Corwin, J.T., and Nevill, G. (1993). Ultrastructural evidence for hair cell regeneration in the mammalian inner ear. Science *259*, 1616–1619.

Forge, A., Li, L., and Nevill, G. (1998). Hair cell recovery in the vestibular sensory epithelia of mature guinea pigs. J. Comp. Neurol. *397*, 69–88.

Gao, Z., Kelly, M.C., Yu, D., Wu, H., Lin, X., Chi, F.L., and Chen, P. (2016). Spatial and age-dependent hair cell generation in the postnatal mammalian utricle. Mol. Neurobiol. *53*, 1601–1612.

Geleoc, G.S., and Holt, J.R. (2003). Developmental acquisition of sensory transduction in hair cells of the mouse inner ear. Nat. Neurosci. *6*, 1019–1020.

Geleoc, G.S., Risner, J.R., and Holt, J.R. (2004). Developmental acquisition of voltage-dependent conductances and sensory signaling in hair cells of the embryonic mouse inner ear. J. Neurosci. *24*, 11148–11159.

Geng, R., Geller, S.F., Hayashi, T., Ray, C.A., Reh, T.A., Bermingham-McDonogh, O., Jones, S.M., Wright, C.G., Melki, S., Imanishi, Y., et al. (2009). Usher syndrome IIIA gene clarin-1 is essential for hair cell function and associated neural activation. Hum. Mol. Genet. *18*, 2748–2760.

Golub, J.S., Tong, L., Ngyuen, T.B., Hume, C.R., Palmiter, R.D., Rubel, E.W., and Stone, J.S. (2012). Hair cell replacement in adult mouse utricles after targeted ablation of hair cells with diphtheria toxin. J. Neurosci. *32*, 15093–15105.

Gomez-Casati, M.E., Murtie, J., Taylor, B., and Corfas, G. (2010). Cell-specific inducible gene recombination in postnatal inner ear supporting cells and glia. J. Assoc. Res. Otolaryngol. *11*, 19–26.

Gubbels, S.P., Woessner, D.W., Mitchell, J.C., Ricci, A.J., and Brigande, J.V. (2008). Functional auditory hair cells produced in the mammalian cochlea by in utero gene transfer. Nature *455*, 537–541.

Jones, T.A. (1992). Vestibular short latency responses to pulsed linear acceleration in unanesthetized animals. Electroencephalogr. Clin. Neurophysiol. *82*, 377–386.

Jones, T.A., and Jones, S.M. (1999). Short latency compound action potentials from mammalian gravity receptor organs. Hear. Res. *136*, 75–85.

Jones, T.A., and Nelson, R.C. (1992). Recovery of vestibular function following hair cell destruction by streptomycin. Hear. Res. *62*, 181–186.

Jones, S.M., Jones, T.A., Bell, P.L., and Taylor, M.J. (2001). Compound gravity receptor polarization vectors evidenced by linear vestibular evoked potentials. Hear. Res. *154*, 54–61.

Jones, T.A., Jones, S.M., Vijayakumar, S., Brugeaud, A., Bothwell, M., and Chabbert, C. (2011). The adequate stimulus for mammalian linear vestibular evoked potentials (VsEPs). Hear. Res. *280*, 133–140.

Kawamoto, K., Izumikawa, M., Beyer, L.A., Atkin, G.M., and Raphael, Y. (2009). Spontaneous hair cell regeneration in the mouse utricle following gentamicin ototoxicity. Hear. Res. *247*, 17–26.

Kelly, M.C., Chang, Q., Pan, A., Lin, X., and Chen, P. (2012). Atoh1 directs the formation of sensory mosaics and induces cell proliferation in the postnatal mammalian cochlea in vivo. J. Neurosci. *32*, 6699–6710.

Kim, K.S., Minor, L.B., Della Santina, C.C., and Lasker, D.M. (2011). Variation in response dynamics of regular and irregular vestibular-nerve afferents during sinusoidal head rotations and currents in the chinchilla. Exp. Brain Res. *210*, 643–649.

Krey, J.F., Krystofiak, E.S., Dumont, R.A., Vijayakumar, S., Choi, D., Rivero, F., Kachar, B., Jones, S.M., and Barr-Gillespie, P.G. (2016). Plastin 1 widens stereocilia by transforming actin filament packing from hexagonal to liquid. J. Cell Biol. *215*, 467–482.

Lanford, P.J., Shailam, R., Norton, C.R., Gridley, T., and Kelley, M.W. (2000). Expression of Math1 and HES5 in the cochleae of wildtype and Jag2 mutant mice. J. Assoc. Res. Otolaryngol. *1*, 161–171.

Lewis, R.M., Hume, C.R., and Stone, J.S. (2012). Atoh1 expression and function during auditory hair cell regeneration in post-hatch chickens. Hear. Res. *289*, 74–85.

Li, L., Nevill, G., and Forge, A. (1995). Two modes of hair cell loss from the vestibular sensory epithelia of the guinea pig inner ear. J. Comp. Neurol. *355*, 405–417.

Lin, V., Golub, J.S., Nguyen, T.B., Hume, C.R., Oesterle, E.C., and Stone, J.S. (2011). Inhibition of Notch activity promotes nonmitotic regeneration of hair cells in the adult mouse utricles. J. Neurosci. *31*, 15329–15339.

Liu, Z., Dearman, J.A., Cox, B.C., Walters, B.J., Zhang, L., Ayrault, O., Zindy, F., Gan, L., Roussel, M.F., and Zuo, J. (2012). Age-dependent in vivo conversion of mouse cochlear pillar and Deiters' cells to immature hair cells by Atoh1 ectopic expression. J. Neurosci. *32*, 6600–6610.

Llorens, J., Soler-Martin, C., Saldana-Ruiz, S., Cutillas, B., Ambrosio, S., and Boadas-Vaello, P. (2011). A new unifying hypothesis for lathyrism, konzo and tropical ataxic neuropathy: nitriles are the causative agents. Food Chem. Toxicol. *49*, 563–570.

Madisen, L., Zwingman, T.A., Sunkin, S.M., Oh, S.W., Zariwala, H.A., Gu, H., Ng, L.L., Palmiter, R.D., Hawrylycz, M.J., Jones, A.R., et al. (2010). A robust and high-throughput Cre reporting and characterization system for the whole mouse brain. Nat. Neurosci. *13*, 133–140.

McGovern, M.M., Brancheck, J., Grant, A.C., Graves, K.A., and Cox, B.C. (2017). Quantitative analysis of supporting cell subtype labeling among CreER lines in the neonatal mouse cochlea. J. Assoc. Res. Otolaryngol. *18*, 227–245.

McInturff, S., Burns, J.C., and Kelley, M.W. (2018). Characterization of spatial and temporal development of type I and type II hair cells in the mouse utricle using new cell-type-specific markers. Biol. Open *7*, bio038083.

Myrdal, S.E., Johnson, K.C., and Steyger, P.S. (2005). Cytoplasmic and intranuclear binding of gentamicin does not require endocytosis. Hear. Res. *204*, 156–169.

Nazareth, A.M., and Jones, T.A. (1998). Central and peripheral components of short latency vestibular responses in the chicken. J. Vestib. Res. *8*, 233–252.

Oshima, K., Shin, K., Diensthuber, M., Peng, A.W., Ricci, A.J., and Heller, S. (2010). Mechanosensitive hair cell-like cells from embryonic and induced pluripotent stem cells. Cell *141*, 704–716.

Roberson, D.F., Weisleder, P., Bohrer, P.S., and Rubel, E.W. (1992). Ongoing production of sensory cells in the vestibular epithelium of the chick. Hear. Res. *57*, 166–174.

Sandoval, R., Leiser, J., and Molitoris, B.A. (1998). Aminoglycoside antibiotics traffic to the Golgi complex in LLC-PK1 cells. J. Am. Soc. Nephrol. *9*, 167–174.

Schlecker, C., Praetorius, M., Brough, D.E., Presler, R.G., Jr., Hsu, C., Plinkert, P.K., and Staecker, H. (2011). Selective atonal gene delivery improves balance function in a mouse model of vestibular disease. Gene Ther. *18*, 884–890.

Shou, J., Zheng, J.L., and Gao, W.Q. (2003). Robust generation of new hair cells in the mature mammalian inner ear by adenoviral expression of Hath1. Mol. Cell. Neurosci. *23*, 169–179.

Soler-Martin, C., Diez-Padrisa, N., Boadas-Vaello, P., and Llorens, J. (2007). Behavioral disturbances and hair cell loss in the inner ear following nitrile exposure in mice, guinea pigs, and frogs. Toxicol. Sci. *96*, 123–132.

Walters, B.J., Coak, E., Dearman, J., Bailey, G., Yamashita, T., Kuo, B., and Zuo, J. (2017). In vivo interplay between p27(Kip1), GATA3, ATOH1, and POU4F3 converts non-sensory cells to hair cells in adult mice. Cell Rep. *19*, 307–320.

Wang, T., Chai, R., Kim, G.S., Pham, N., Jansson, L., Nguyen, D.H., Kuo, B., May, L.A., Zuo, J., Cunningham, L.L., et al. (2015). Lgr5+ cells regenerate hair cells via proliferation and direct transdifferentiation in damaged neonatal mouse utricle. Nat. Commun. *6*, 6613.

Wang, T., Niwa, M., Sayyid, Z.N., Hosseini, D.K., Pham, N., Jones, S.M., Riccie, A.J., and Cheng, A.G. (2019). Uncoordinated maturation of developing and regenerating postnatal mammalian vestibular hair cells. PLoS Biol. *17*, e3000326.

Warchol, M.E., Lambert, P.R., Goldstein, B.J., Forge, A., and Corwin, J.T. (1993). Regenerative proliferation in inner ear sensory epithelia from adult guinea pigs and humans. Science *259*, 1619–1622.

Weisleder, P., and Rubel, E.W. (1992). Hair cell regeneration in the avian vestibular epithelium. Exp. Neurol. *115*, 2–6.

Weisleder, P., Jones, T.A., and Rubel, E.W. (1990). Peripheral generators of the vestibular evoked potentials (VsEPs) in the chick. Electroencephalogr. Clin. Neurophysiol. *76*, 362–369.

Yamashita, T., Zheng, F., Finkelstein, D., Kellard, Z., Carter, R., Rosencrance, C.D., Sugino, K., Easton, J., Gawad, C., and Zuo, J. (2018). High-resolution transcriptional dissection of in vivo Atoh1-mediated hair cell conversion in mature cochleae identifies Isl1 as a co-reprogramming factor. PLoS Genet. *14*, e1007552.

Yang, S.M., Chen, W., Guo, W.W., Jia, S., Sun, J.H., Liu, H.Z., Young, W.Y., and He, D.Z. (2012). Regeneration of stereocilia of hair cells by forced Atoh1 expression in the adult mammalian cochlea. PLoS ONE *7*, e46355.

Zheng, F., and Zuo, J. (2017). Cochlear hair cell regeneration after noise-induced hearing loss: Does regeneration follow development? Hear. Res. *349*, 182–196.

STAR★METHODS

KEY RESOURCES TABLE

REAGENT or RESOURCE	SOURCE	IDENTIFIER
Antibodies		
Myosin7a	Proteus Biosciences	Cat Num 25-6790; RRID:AB_2314839
Myosin7a	DSHB	Cat Num MYO7A 138-1; RRID:AB_2282417
Sox2	Santa Cruz Biotechnology	Cat Num sc-17320; RRID:AB_2286684
AnnexinA4	R&D Systems	Cat Num AF4146; RRID:AB_2242796
Osteopontin	R&D Systems	Cat Num AF808; RRID:AB_2194992
Tuj1	Neuromics	Cat Num MO15013; RRID:AB_2737114
Neurofilament	Abcam	Cat Num ab4680; RRID:AB_304560
Ctbp2	BD Transduction Laboratories	Cat Num 612044; RRID:AB_399431
Shank1	Santa Cruz Biotechnology	Cat Num sc-23543; RRID:AB_2301736
Ki67	Abcam	Cat Num ab16667; RRID:AB_302459
Atoh1	Proteintech	Cat Num 21215-1-AP; RRID:AB_10733126
HA	Sigma-Aldrich	Cat Num ab9110; RRID:AB_307019
Alexa Fluor donkey anti-goat 488	Thermo Fisher Scientific	Cat Num A11055; RRID:AB_2534102
Alexa Fluor donkey anti-goat 546	Thermo Fisher Scientific	Cat Num A11056; RRID:AB_142628
Alexa Fluor donkey anti-goat 647	Thermo Fisher Scientific	Cat Num A21447; RRID:AB_141844
Alexa Fluor donkey anti-mouse 488	Thermo Fisher Scientific	Cat Num A21202; RRID:AB_141607
Alexa Fluor donkey anti-mouse 546	Thermo Fisher Scientific	Cat Num A10036; RRID:AB_2534012
Alexa Fluor donkey anti-mouse 647	Thermo Fisher Scientific	Cat Num A31571; RRID:AB_162542
Alexa Fluor donkey anti-rabbit 488	Thermo Fisher Scientific	Cat Num A21206; RRID:AB_2535792
Alexa Fluor donkey anti-rabbit 546	Thermo Fisher Scientific	Cat Num A10040; RRID:AB_2534016
Alexa Fluor donkey anti-rabbit 647	Thermo Fisher Scientific	Cat Num A31573; RRID:AB_2536183
Phalloidin	Thermo Fisher Scientific	Cat Num A22287; RRID:AB_2620155
DAPI	Thermo Fisher Scientific	Cat Num D1306; RRID:AB_2629482
Chemicals, Peptides, and Recombinant Proteins		
3,3′-iminodipropionitrile	Pfaltz & Bauer	#I00455
Tamoxifen	Sigma-Aldrich	#T5648-1G
EdU	Thermo Fisher Scientific	#A10044
NaOH	Thermo Fisher Scientific	S318-500
Tris-HCl	Thermo Fisher Scientific	#15568025
Ketamine	Vedco	#NDC 50989-161-06
Xylazine	Santa Cruz Animal Health	#SC-36294Rx
Critical Commercial Assays		
Alexa Fluor 647 EdU Detection Kit	Thermo Fisher Scientific	#C10340
Experimental Models: Organisms/Strains		
Mouse: B6.Cg-Tg(Plp1-cre/ERT)3Pop/J	Jackson Laboratory	RRID:IMSR_JAX:005975
Mouse: B6;129S6-Gt(ROSA)26Sortm14(CAG-tdTomato)Hze/J	Jackson Laboratory	RRID:IMSR_JAX:007908
Mouse: CAG-flox-Atoh1-HA	Liu et al., 2012	n/a
Mouse: Crl:CD1(ICR)	Charles River	RRID:IMSR_CRL:22
Oligonucleotides		
5′-ACGCTCTGTCGGAGTTGCTG-3′	n/a	Atoh1-HA transgene (forward)
5′-AGGGATAGCCCGCATAGTCA-3′	n/a	Atoh1-HA transgene (reverse)
5′-CTAGGCCACAGAATTGAAAGATCT-3′	n/a	Plp1-Cre internal positive control (forward)
5′-GTAGGTGGAAATTCTAGCATCC-3′	n/a	Plp1-Cre internal positive control (reverse)

(*Continued on next page*)

Continued		
REAGENT or RESOURCE	SOURCE	IDENTIFIER
5′-GCGGTCTGCCAGTAAAAACTATC-3′	n/a	Plp1-Cre transgene (forward)
5′-GTGAAACAGCATTGCTGTCACTT-3′	n/a	Plp1-Cre transgene (reverse)
5′- CTGTTCCTGTACGGCATGG −3′	n/a	tdTomato mutant (forward)
5′- GGCATTAAAGCAGCGTATCC −3′	n/a	tdTomato mutant (reverse)
5′-AAGGGAGCTGCAGTGGAGTA-3′	n/a	tdTomato wild type (forward)
5′-CCGAAAATCTGTGGGAAGTC-3′	n/a	tdTomato wild type (reverse)
Software and Algorithms		
Fiji v2.0.0	NIH	n/a
GraphPad Prism v7.0c	GraphPad	n/a
RStudio v0.99.891	RStudio, Inc.	n/a
Other		
PBS	Sigma-Aldrich	#T5648-1G
BSA	Thermo Fisher Scientific	#BP1600-100
NaN_3	Sigma-Aldrich	#S2002-25G
DAKO	Agilent	#S3023

LEAD CONTACT AND MATERIALS AVAILABILITY

Further information and requests for resources and reagents should be directed to and will be fulfilled by the Lead Contact, Alan Cheng (aglcheng@stanford.edu).

EXPERIMENTAL MODEL AND SUBJECT DETAILS

Mice

Plp1-CreERT (Jackson Laboratory, RRID:IMSR_JAX:005975, Bar Harbor, Maine, USA) (Doerflinger et al., 2003; Gomez-Casati et al., 2010; Madisen et al., 2010), *Rosa26-tdTomato* (Jackson Laboratory, RRID:IMSR_JAX:007908, Bar Harbor, Maine, USA) (Madisen et al., 2010), *CAG-flox-Atoh1-HA* (gift of J. Zuo, Creighton University, Omaha, Nebraska, USA) (Liu et al., 2012), and wild-type CD1 (Charles River, RRID:IMSR_CRL:22, Wilmington, Massachusetts, USA) mice of both sexes were used. Littermates were group housed under standard husbandry conditions and were randomly assigned to experimental groups. All animals were confirmed to be in good health and not involved in previous procedures. Genotypes of experimental animals included: wild-type CD1, $Plp1^{CreERT/+}$; $Rosa26^{tdTomato/+}$, $Plp1^{CreERT/+}$; $CAG^{flox\text{-}Atoh1\text{-}HA/+}$, and $Plp1^{CreERT/+}$; $CAG^{flox\text{-}Atoh1\text{-}HA/+}$; $Rosa26^{tdTomato/+}$. IDPN (3,3′-iminodipropionitrile; Pfaltz & Bauer, #I00455, Waterbury, Connecticut, USA) was injected intraperitoneally (IP, 2-6 mg/g) once for adult mice (P30). Tamoxifen (dissolved in corn oil; #T5648-1G, Sigma-Aldrich, St. Louis, Missouri, USA) (IP, 9 mg/40 g) and EdU (IP, 1 mg/kg, Thermo Fisher Scientific, #A10044, Waltham, Massachusetts, USA) were used in a subset of mice. Mortality was low (< 5%) with the use of multiple drugs (4 mg/g IDPN, tamoxifen, EdU) in transgenic (Plp1-Atoh1-HA) animals. Mortality was ~50% when 6 mg/g IDPN was used. No significant differences in either the degree of damage induced by IDPN or subsequent regeneration were observed between ears or between sexes (data not shown). All protocols conform to relevant regulatory standards and were approved by the Animal Care and Use Committee of the Stanford University School of Medicine and NIH.

METHOD DETAILS

Genotyping

Genomic DNA of transgenic mice was collected to perform PCRs. DNA was isolated by adding 180 μL of 50 mM sodium hydroxide (NaOH, Thermo Fisher Scientific, S318-500) to ear biopsies, incubating at 98°C for 1 hour, then adding 20 μL of 1 M Tris-HCl (Invitrogen, Thermo Fisher Scientific, #15568025). A list of primers and sequences used for genotyping can be found in the Key Resources Table.

Vestibular physiology

Linear vestibular evoked potential (VsEP) responses were recorded from mice at various ages (P37, P60, P120, P210) as previously described (Jones and Jones, 1999). Briefly, mice were first anesthetized with a 1:1 cocktail of ketamine (100 mg/kg, #NDC 50989-161-06, Vedco, St. Joseph, Missouri, USA) and xylazine (10 mg/kg, #SC-36294Rx, Santa Cruz Animal Health, Dallas, TX, USA).

Rectal temperatures were maintained at 37°C, and electrocardiographic (ECG) activity was monitored using an oscilloscope. Subcutaneous stainless-steel electrodes were placed over the caudal cerebrum (non-inverting electrode), subcutaneously behind the right pinna (inverting electrode), and intramuscularly in the right thigh muscle (ground electrode). A head clip was used to secure the head to the mechanical shaker, which was used to deliver linear vestibular stimuli in the naso-occipital axis. Vertical motion of the shaker was monitored with an accelerometer and adjusted to produce the stimulus waveforms. Throughout the study, jerk stimuli ranging from 0.125 g/ms to 2.0 g/ms were provided (Jones et al., 2011). Signals were amplified (200,000x), filtered (low filter = 300 Hz, high filter = 3000 Hz), and digitized via an analog-to-digital (A/D) converter for all VsEP recordings. Responses from normal and inverted stimulus polarities were collected and added together for a total of 256 sweeps for each waveform. A masker (90 dB SPL; bandwidth 50 Hz to 50 kHz) from a free-field speaker driver was used to prevent responses from the auditory components of cranial nerve VIII. All responses were blindly analyzed for three components: threshold (g/ms), P1 latency (ms) and P1-N1 amplitude (μV). Thresholds were defined as the average stimulus intensity between the lowest stimulus intensity at which a response was observed and the following stimulus intensity that failed to elicit a response. Latencies were measured relative to the onset of the stimulus for the first positive response peak (P1). Amplitudes represented peak-to-peak magnitudes between P1 and N1. Whereas the first positive and negative response peaks (P1 and N1, respectively) reflect activity of the peripheral vestibular nerve, peaks beyond N1 reflect activity of the brainstem and central vestibular relays (Jones, 1992; Nazareth and Jones, 1998).

Immunohistochemistry

After microdissection from the temporal bone, utricles were fixed in 4% paraformaldehyde (in PBS, pH 7.4; Electron Microscopy Services, #15710, Hatfield, Pennsylvania, USA) for 40 min at room temperature. Tissues were then washed with PBS 3 times for at least 5 minutes each, then blocked with 5% donkey serum, 0.1% Triton X-100, 1% bovine serum albumin (BSA, Thermo Fisher Scientific, #BP1600-100), and 0.02% sodium azide (NaN_3, Sigma-Aldrich, #S2002-25G) in PBS at pH 7.4 for 1 hour at room temperature. Primary antibodies diluted in the same blocking solution were added overnight at 4°C. The following day, after washing with PBS, tissues were incubated with secondary antibodies diluted in 0.1% Triton X-100, 0.1% BSA, and 0.02% NaN_3 solution in PBS at pH 7.4 for 2 hours at room temperature. After washing with PBS, tissues were mounted with antifade Fluorescence Mounting Medium (DAKO, Agilent, #S3023, Santa Clara, California, USA) and coverslipped. Antibodies against the following proteins were used: Myosin7a (1:1000, rabbit, RRID:AB_2314839, Proteus Biosciences, Ramona, California, USA), Myosin7a (1:500, mouse, DSHB, RRID:AB_2282417, Iowa City, Iowa, USA), Sox2 (1:400, goat, RRID:AB_2286684, Santa Cruz Biotechnology, Santa Cruz, California, USA), AnnexinA4 (1:200, goat, RRID:AB_2242796, R&D Systems, Minneapolis, Minnesota, USA), Osteopontin (1:200, goat, RRID:AB_2194992, R&D Systems), Tuj1 (1:1000, mouse, Neuromics, RRID:AB_2737114, Edina, Minnesota, USA), Neurofilament (1:1000, chicken, Abcam, RRID:AB_304560, Cambridge, United Kingdom), Ctbp2 (1:1000, mouse, RRID:AB_399431, BD Transduction Laboratories, Franklin Lakes, New Jersey, USA), Shank1 (1:1000, goat, RRID:AB_2301736, Santa Cruz Biotechnology), Ki67 (1:500, rabbit, RRID:AB_302459, Abcam, Cambridge, United Kingdom), Atoh1 (1:2000, rabbit, RRID:AB_10733126, Proteintech, Rosemont, Illinois, USA) (Atkinson et al., 2018), and HA (1:500, rabbit, RRID:AB_307019, Sigma-Aldrich). Secondary antibodies included Alexa Fluor donkey anti-goat 488 (RRID:AB_2534102), Alexa Fluor donkey anti-goat 546 (RRID:AB_142628), Alexa Fluor donkey anti-goat 647 (RRID:AB_141844), Alexa Fluor donkey anti-mouse 488 (RRID:AB_141607), Alexa Fluor donkey anti-mouse 546 (RRID:AB_2534012), Alexa Fluor donkey anti-mouse 647 (RRID:AB_162542), Alexa Fluor donkey anti-rabbit 488 (RRID:AB_2535792) Alexa Fluor donkey anti-rabbit 546 (RRID:AB_2534016), Alexa Fluor donkey anti-rabbit 647 (RRID:AB_2536183, all Thermo Fisher Scientific) at 1:250 to 1:500. Fluorescence-conjugated phalloidin (1:1,000; RRID:AB_2620155, Thermo Fisher Scientific), DAPI (1:10,000 from 5mg/ml stock solution; RRID:AB_2629482, Thermo Fisher Scientific), and Alexa Fluor 647 EdU Detection Kit (#C10340, Thermo Fisher Scientific) were used. Texas Red-conjugated gentamicin (GTTR) was synthesized as previously described and applied at 1:200 of stock solution (0.85 mg/mL) for 2 hours (Myrdal et al., 2005; Sandoval et al., 1998).

QUANTIFICATION AND STATISTICAL ANALYSIS

Image acquisition and cell quantification

Low-magnification images were acquired using epifluorescent microscopy (Axioplan 2, Zeiss, Oberkochen, Germany). High-magnification Z stack images were captured using a 63x objective on a Zeiss LSM 700 or 880 confocal microscope (Zen Black, Zeiss). Whole utricle images were acquired using tile scanning via Z-stack images tiled across the length and width of the entire utricle at 63x magnification on the Zeiss LSM 880 confocal microscope. Once the image was captured with Zen Black, it was transferred to Zen Blue for image processing. The image was then stitched during post-processing to fuse the individual tiles. From these Z stack images, cell quantification was performed either per 10,000 μm^2 or per organ using Fiji software (v2.0.0, NIH, Bethesda, Maryland, USA). Cell counts were analyzed either from 1-2 representative areas from the extrastriola and striola, or from merged images spanning the whole utricle (merged together using Zeiss Zen software). Quantification of total HC numbers represents cell counts from the entire sensory epithelium. For all experiments, *n* values represent the number of animals or utricles or cells examined.

Statistical analyses

Statistical analyses were conducted using GraphPad Prism (v7.0c software, GraphPad, San Diego, CA, USA) and RStudio (v0.99.891, RStudio, Inc., Boston, MA, USA). Statistical significance was determined using χ^2 tests, Student's t tests, or one- or two-way ANOVA followed by post hoc analysis via Tukey's multiple comparisons test unless otherwise stated as appropriate. A p value less than 0.05 was considered significant: *$p < 0.05$, **$p < 0.01$, ***$p < 0.001$. Data are shown as mean ± s.d. Linear regression analysis was performed to quantify goodness of fit via computation of the Pearson correlation coefficient (RStudio). Details of experiments can be found in the figures and figure legends. Numbers of animals, utricles, or HCs listed in parentheses.

Cell Reports, Volume *28*

Supplemental Information

Atoh1 Directs Regeneration and Functional Recovery of the Mature Mouse Vestibular System

Zahra N. Sayyid, Tian Wang, Leon Chen, Sherri M. Jones, and Alan G. Cheng

Supplementary Materials

Figure S1

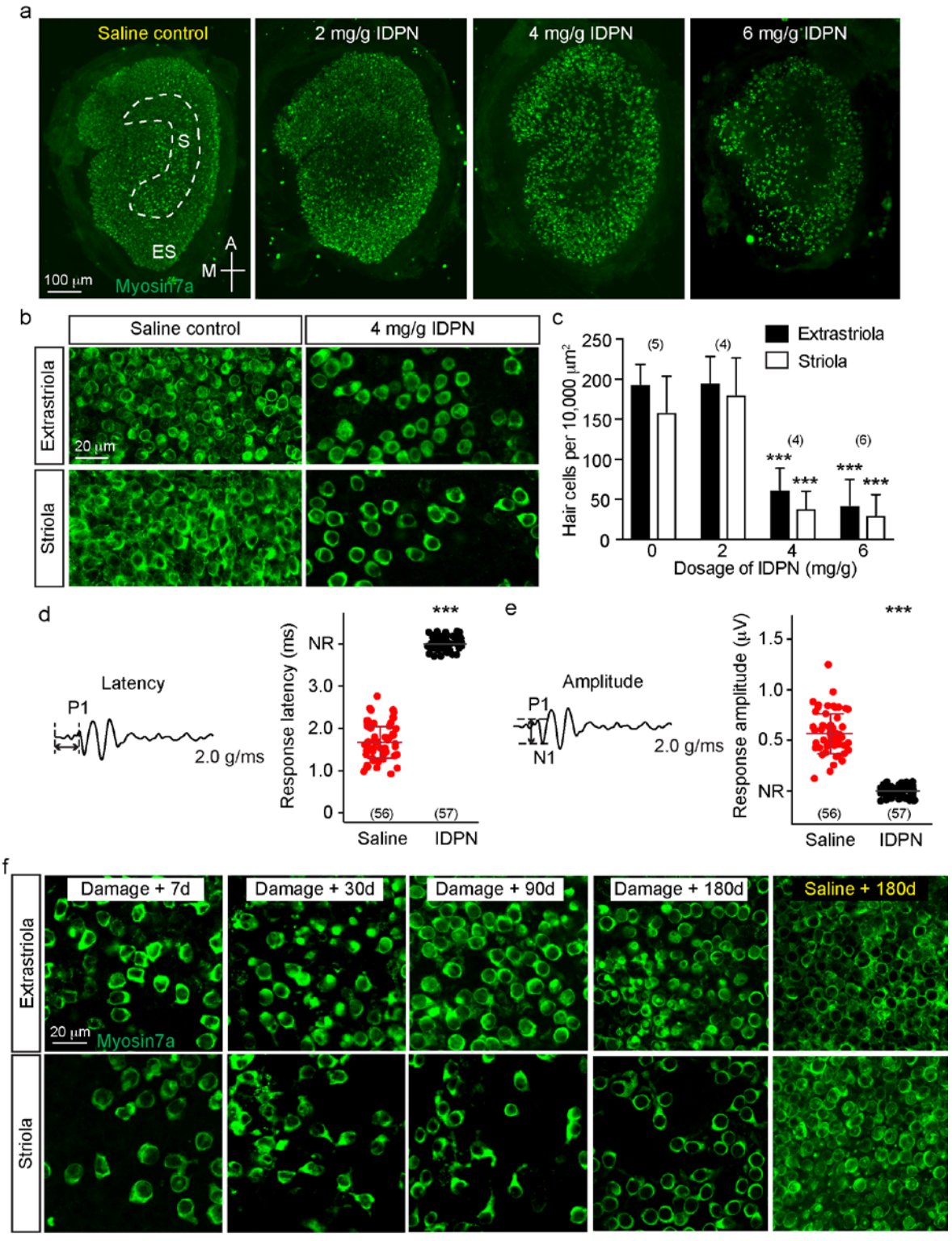
a
Saline control
2 mg/g IDPN
4 mg/g IDPN
6 mg/g IDPN
S
ES
A
M
100 μm
Myosin7a
b
Saline control
4 mg/g IDPN
Extrastriola
Striola
20 μm
c
Extrastriola
Striola
Hair cells per 10,000 μm²
Dosage of IDPN (mg/g)
(5)
(4)
(4)
(6)
***
d
Latency
P1
2.0 g/ms
Response latency (ms)
NR
(56)
(57)
Saline
IDPN
e
Amplitude
P1
N1
2.0 g/ms
Response amplitude (μV)
f
Damage + 7d
Damage + 30d
Damage + 90d
Damage + 180d
Saline + 180d
Extrastriola
Striola
20 μm
Myosin7a

Supplemental Figure 1. Model of hair cell degeneration and regeneration (related to Figure 1). (a) IDPN (P30) caused a dose-dependent loss of HCs seven days later in wildtype mice *in vivo*. Dashed lines outline the striolar region. (b) Representative high magnification, confocal images of the extrastriolar and striolar regions showing HC loss in the IDPN damaged utricles as compared to undamaged controls. (c) Myosin7a^{+} cell counts showing significant HC loss in the extrastriolar and striolar regions at doses 4 mg/g or higher. A moderate dose (4 mg/g) was selected for use hereon, as the higher dose (6 mg/g) increased morbidity and mortality of mice. (d-e) Representative VsEP traces denoting P1 latency and P1-N1 amplitude in highest input stimulus (2.0 g/ms). IDPN-treated animals displayed significantly longer latencies and smaller amplitudes than undamaged controls. (f) Representative high magnification images showing HC loss, with regeneration primarily in the extrastriolar region. Two-way ANOVA with Dunnett's multiple comparisons test (c), two-way Student's t-tests for (d-e), n for utricles (c) or animals (d-e). * in (e) refers to comparisons to the 0 mg/kg dose.

Figure S2

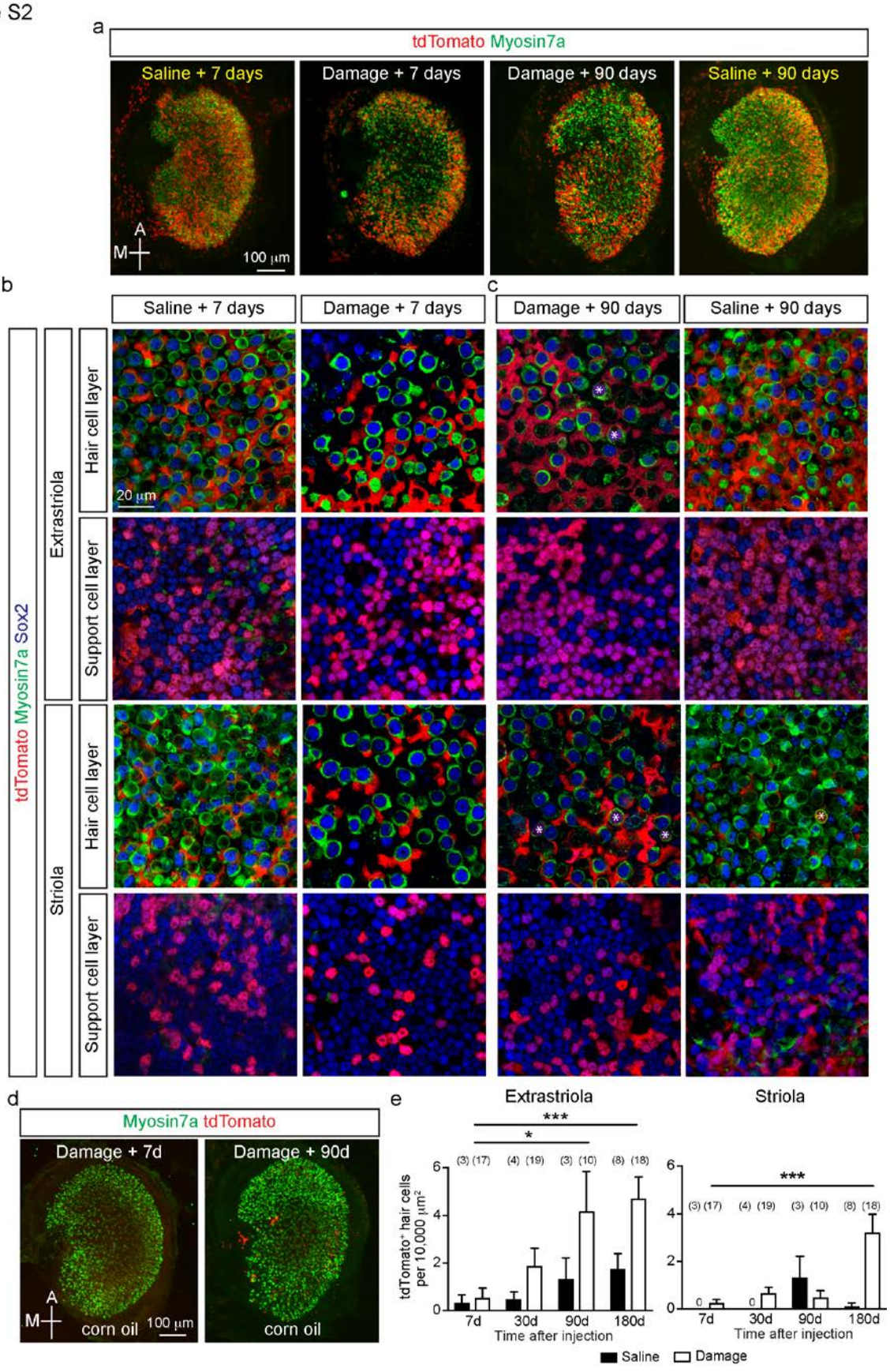
a
tdTomato Myosin7a
Saline + 7 days
Damage + 7 days
Damage + 90 days
Saline + 90 days
A
M
100 μm
b
c
tdTomato Myosin7a Sox2
Extrastriola
Striola
Hair cell layer
Support cell layer
20 μm
d
Myosin7a tdTomato
Damage + 7d
Damage + 90d
corn oil
e
Extrastriola
Striola
tdTomato+ hair cells per 10,000 μm2
Time after injection
7d
30d
90d
180d
Saline
Damage

Supplemental Figure 2. Lineage tracing of support cells in the mature mouse utricle (related to Figure 1). (a) P32 $Plp1^{CreERT/+}$; $R26^{tdTomato/+}$ mice were administered tamoxifen. Cre recombination occurs primarily in the extrastriolar regions of the damaged and undamaged adult mouse utricles. (b) Representative high magnification images showing loss of HCs and tdTomato-labeling of support cells in both the extrastriolar and striolar regions seven days post treatment with saline or IDPN. The extrastriolar region displayed more robust tdTomato-labeling than the striolar region. (c) Ninety days post IDPN or saline treatment, many $tdTomato^+$ support cells and few fate-mapped, $tdTomato^+$, $Myosin7a^+$ HCs were identified (asterisks). (d) Mice treated with IDPN at P30 and vehicle control (corn oil at P32) had minimal Cre recombination (<1%) at both seven and 90 days post treatment, indicating low Cre recombinase leakiness. (e) Quantification shows significant increases in traced, $tdTomato^+$, $Myosin7a^+$ HCs in both the extrastriolar and striolar regions after IDPN-induced damage. Two-way ANOVA with Tukey's multiple comparisons test, n for utricles.

Figure S3

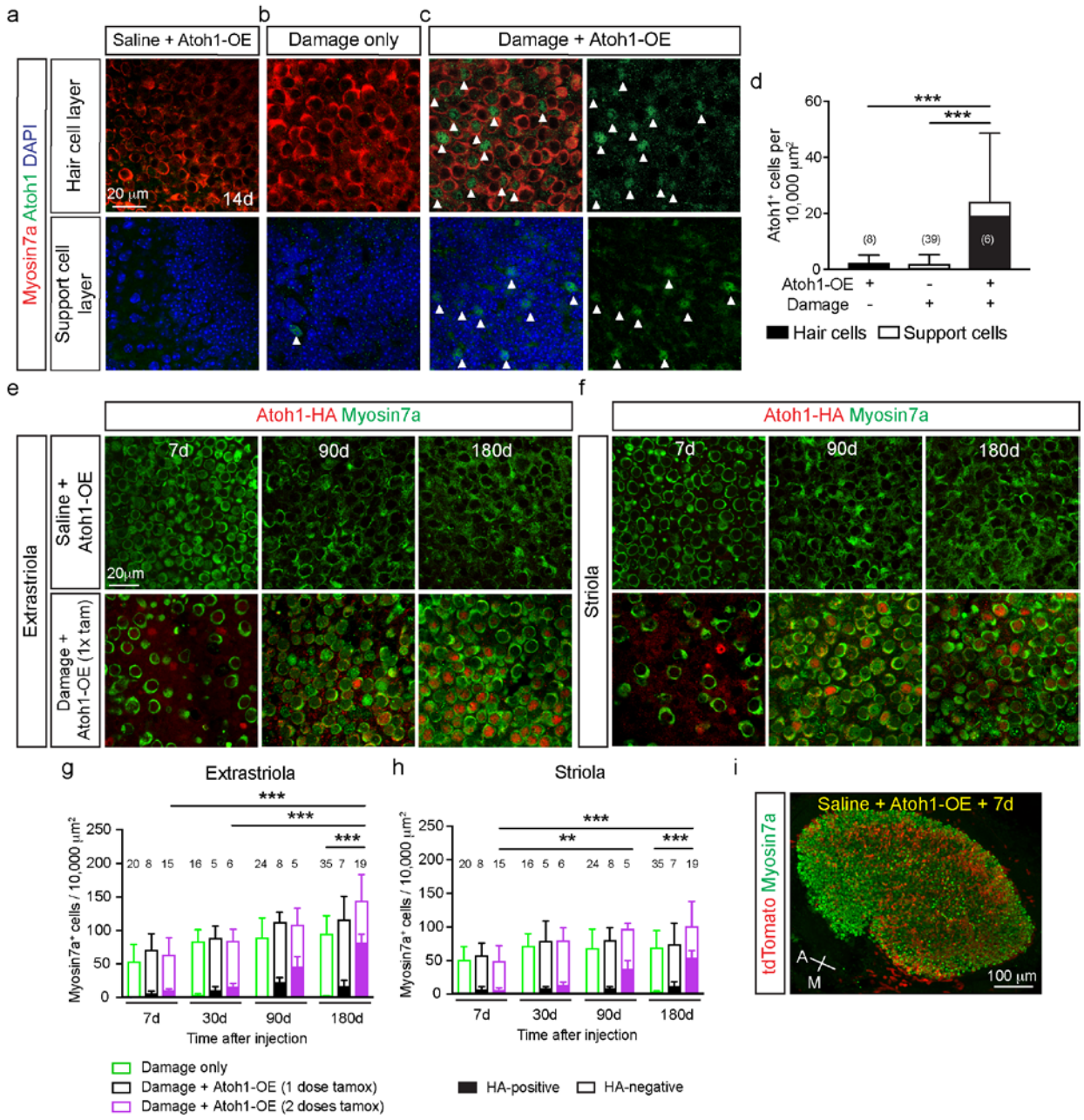

Supplemental Figure 3. Tamoxifen dosage affects the degree of Atoh1 OE in the damaged utricle (related to Figure 2). (a) With saline administration and Atoh1 OE, immunolabeling with Atoh1 antibody showed that Atoh1$^+$ cells (green) were almost always absent in the sensory epithelium at 14 days. (b) Rare Atoh1$^+$ cells were labeled 14 days after damage only (arrowheads). (c) Many Atoh1$^+$ HCs and support cells were

detected via antibody staining 14 days after damage and Atoh1 OE (arrowheads). (d) Quantification of Atoh1$^+$ cells shows significantly more Atoh1$^+$ cells in Atoh1 OE, damaged utricles than either damage-only or Atoh1 OE, undamaged organs. (e) Representative images of the extrastriolar region seven to 180 days after saline and Atoh1 OE or IDPN and one dose of tamoxifen to overexpress Atoh1. No HA$^+$ cells (red) were identified in the undamaged tissues. Myosin7a$^+$/HA$^+$ HCs were only detected in utricles after damage and Atoh1 OE, where more Myosin7a$^+$ HCs were found at 180 days post treatment. (f) Representative images of the striolar region from Atoh1 OE, undamaged and Atoh1 OE, damaged utricles at defined time points after treatment. No HA$^+$ cells were identified in the undamaged tissues. Myosin7a$^+$/HA$^+$ HCs gradually increased and more Myosin7a$^+$ HCs were noted at 90 and 180 days after damage and Atoh1 OE. (g) Quantification of extrastriolar HC density in damage-only, Atoh1 OE, damaged (single dose of tamoxifen), and Atoh1 OE, damaged (two doses of tamoxifen) tissues. HC density gradually increased after IDPN-induced damage. In the extrastriolar region, HC density is significantly higher in Atoh1 OE, damaged tissues (two doses of tamoxifen) than damage-only ones at 180 days after damage. HA$^+$ HCs gradually increased after damage and Atoh1 OE. (h) Quantification of HC density in the striolar region from damage-only, Atoh1 OE, damaged (single dose of tamoxifen), and Atoh1 OE, damaged (two doses of tamoxifen) tissues. HC density gradually increased only after IDPN-induced damage with two doses of tamoxifen to induce Atoh1 OE. Striolar HC density is significantly higher in Atoh1 OE, damaged tissues than damage-only ones at 180 days after damage. Traced HA$^+$ HCs in the striolar region also increased over time after damage and Atoh1 OE. (i) Robust tdTomato expression in undamaged

utricles from *Plp1*$^{CreERT/+}$*; R26*$^{tdTomato/+}$*; CAG*$^{Atoh1\text{-}HA/+}$ mice treated with saline and tamoxifen. One-way ANOVA with Tukey's multiple comparisons test (d), two-way ANOVA with Tukey's multiple comparisons test (f, h), n for utricles.

Figure S4

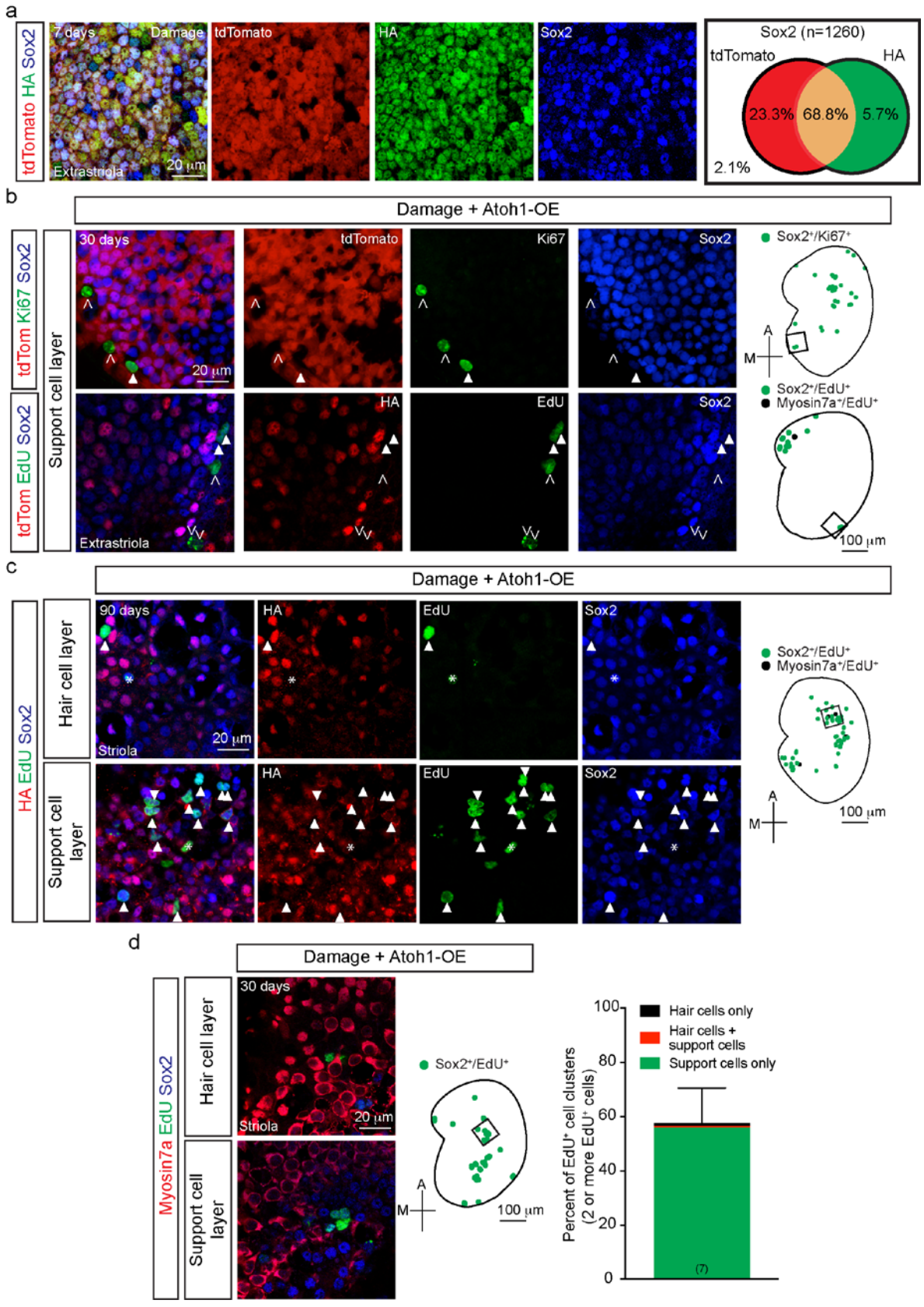
a
tdTomato HA Sox2
7 days
Damage
Extrastriola
20 μm
tdTomato
HA
Sox2
Sox2 (n=1260)
tdTomato
HA
23.3%
68.8%
5.7%
2.1%
b
Damage + Atoh1-OE
tdTom Ki67 Sox2
tdTom EdU Sox2
Support cell layer
30 days
tdTomato
Ki67
Sox2
HA
EdU
Extrastriola
20 μm
Sox2+/Ki67+
Sox2+/EdU+
Myosin7a+/EdU+
A
M
100 μm
c
Damage + Atoh1-OE
HA EdU Sox2
Hair cell layer
Support cell layer
90 days
HA
EdU
Sox2
Striola
20 μm
Sox2+/EdU+
Myosin7a+/EdU+
A
M
100 μm
d
Damage + Atoh1-OE
Myosin7a EdU Sox2
Hair cell layer
Support cell layer
30 days
Striola
20 μm
Sox2+/EdU+
A
M
100 μm
Hair cells only
Hair cells + support cells
Support cells only
Percent of EdU+ cell clusters (2 or more EdU+ cells)
100
80
60
40
20
0
(7)

Supplemental Figure 4. Atoh1 OE increased proliferation in the damaged mature mouse utricle (related to Figure 2). (a) Representative images of support cells from *Plp1*$^{CreERT/+}$*; R26*$^{tdTomato/+}$*; CAG*$^{Atoh1\text{-}HA/+}$ mouse utricle after IDPN and tamoxifen administration. Nearly 70% of Sox2$^+$ support cells in the extrastriolar region were doubled labeled with tdTomato and HA. (b) Ki67$^+$ and EdU$^+$ support cells were detected in the extrastriolar region 30 days after damage and Atoh1 OE. Arrowheads and chevrons indicate Sox2-positive and -negative proliferative (Ki67$^+$ or EdU$^+$) cells. Drawings of utricles show location of proliferative Sox2-positive (green) and Myosin7a-positive cells (black), with black boxes representing areas in the extrastriolar regions where high magnification images were captured. (c) Ninety days after damage and Atoh1 OE, many EdU$^+$ cells were detected in the striolar region, consisting of many EdU$^+$/Sox2$^+$/Myosin7a$^-$ support cells (arrowheads) and a few EdU$^+$/Sox2$^+$/Myosin7a$^+$ HCs (asterisks). Cartoon shows EdU$^+$/Sox2$^+$ (green) and EdU$^+$/Myosin7a$^+$ (black) cells. The black box outlines area in the striolar region where high magnification images were captured. This is the same utricle as shown in Figure 4f. Note that none of the EdU$^+$ cells are HA$^+$. (d) A cluster of EdU$^+$ cells was identified spanning the HC layer and support cell layer of the utricular sensory epithelium 30 days after damage and Atoh1 OE. Cartoon shows EdU$^+$/Sox2$^+$ (green) cells. Among the utricles treated with IDPN and Atoh1 OE, most (58.1%) proliferating cells appeared in foci (two or more cells directly adjacent to one another). Nearly all of these clusters consist of groups of support cells. We rarely found collections of EdU$^+$ support cells adjacent to EdU$^+$ HCs or clusters of EdU$^+$ HCs. N for utricles.

Figure S5

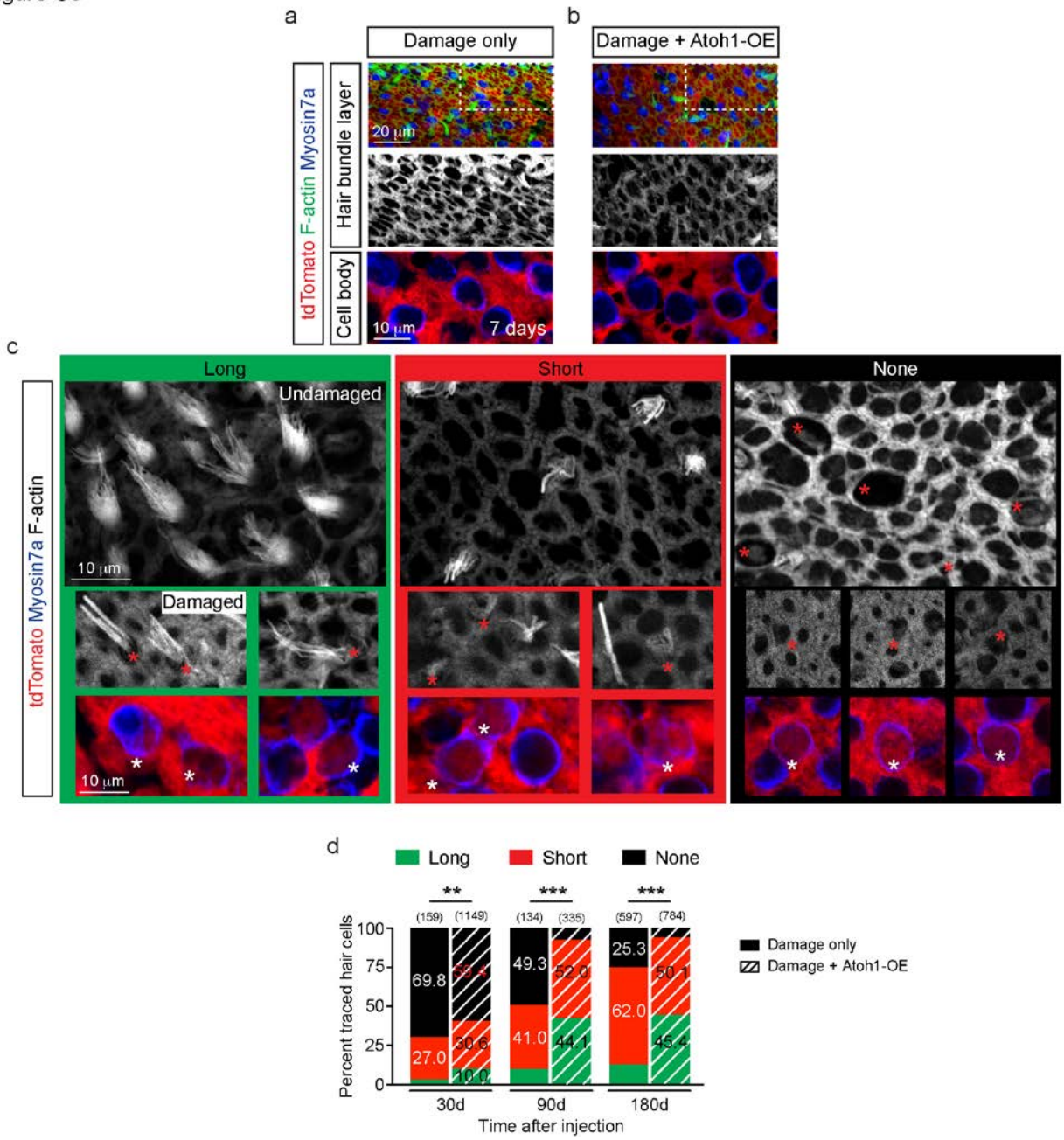

Supplemental Figure 5. Atoh1 OE promotes stereociliary bundle formation in the damaged mature utricle (related to Figure 3). (a-b) Seven days after damage only (a) and damage and Atoh1 OE (b), the apical surface of utricles was largely devoid of stereociliary bundles, and no tdTomato^{+}/Myosin7a^{+} HCs were identified. Dashed boxes represent area from which high magnification images at the hair bundle and cell body

levels are shown. (c) Representative areas depicting long (green), short (red), and no (black) hair bundles. Select traced HCs (asterisks) with associated bundles among the three bundle groups. Lower magnification image of long hair bundles were captured from undamaged utricle, images of short and no bundles were taken from damaged utricles. (d) Quantitative analyses showing the proportion of fate-mapped, tdTomato^{+} HCs with long, short, and no associated stereociliary bundles in damage-only utricles and in Atoh1 OE, damaged utricles. 30 days after damage, most traced HCs had no associated bundles. Bundles detected on traced HCs were primarily short in damage-only and Atoh1 OE, damaged utricles. The proportion of traced cells with long and short bundles 30 days after damage and Atoh1 OE was comparable to that with damage alone. By 90-180 days, nearly 100% of traced HCs after damage and Atoh1 OE had associated bundles, significantly more of which appeared long and thus more mature than those from damage-only utricles. χ^2 test, n for HCs.

Figure S6

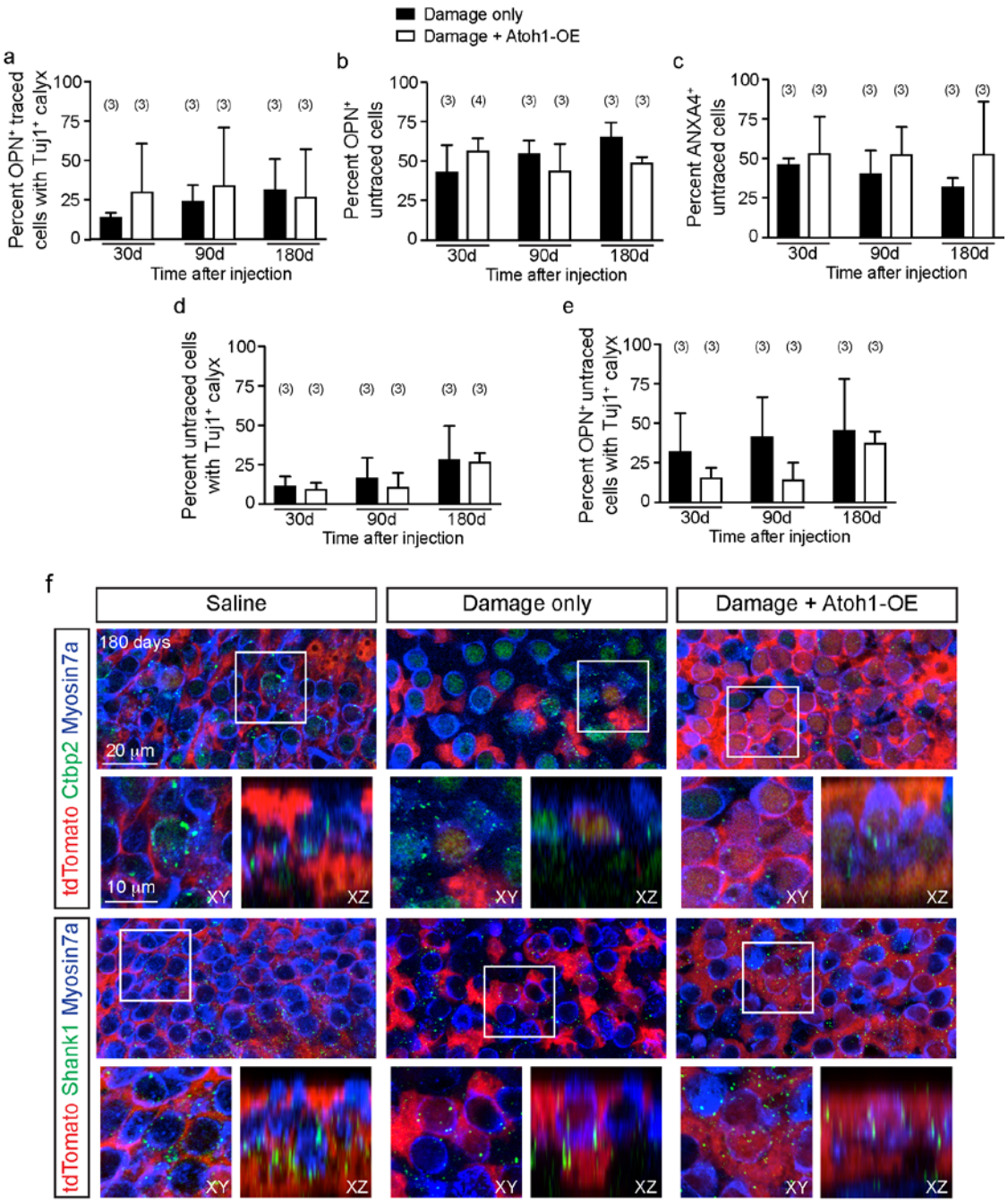

Supplemental Figure 6. Atoh1 increases regeneration of neurally integrated type II hair cells (related to Figure 4). (a) Quantification of traced OPN$^+$ HCs with Tuj1$^+$ calyces

showing no significant change in damage-only and Atoh1 OE, damaged utricles over time. (b-c) Quantification of untraced tdTomato$^-$, Myosin7a$^+$ HCs shows that the percentage of tdTomato$^-$, Myosin7a$^+$ HCs expressing OPN and ANXA4 remain relatively stable over time in both damage-only and Atoh1 OE, damaged utricles, with no significant differences across time points or genotypes. (d) Quantification of untraced tdTomato$^-$, Myosin7a$^+$ HCs with Tuj1$^+$ calyces shows an increase (albeit not statistically significant) in tdTomato$^-$, Myosin7a$^+$ HCs over time in both damage-only and Atoh1 OE, damaged utricles. (e) Quantification of untraced OPN$^+$ HCs with a Tuj1$^+$ calyx showing no significant change in damage-only and Atoh1 OE, damaged utricles over time. (f) Representative images of utricles 180 days after saline, damage only, and damage and Atoh1 OE. The white box outlines area where higher magnification images were captured showing representative traced and untraced HCs expressing presynaptic (Ctbp2) and postsynaptic (Shank1) markers. Two-way ANOVA with Tukey's multiple comparisons test, n for utricles.

Figure S7

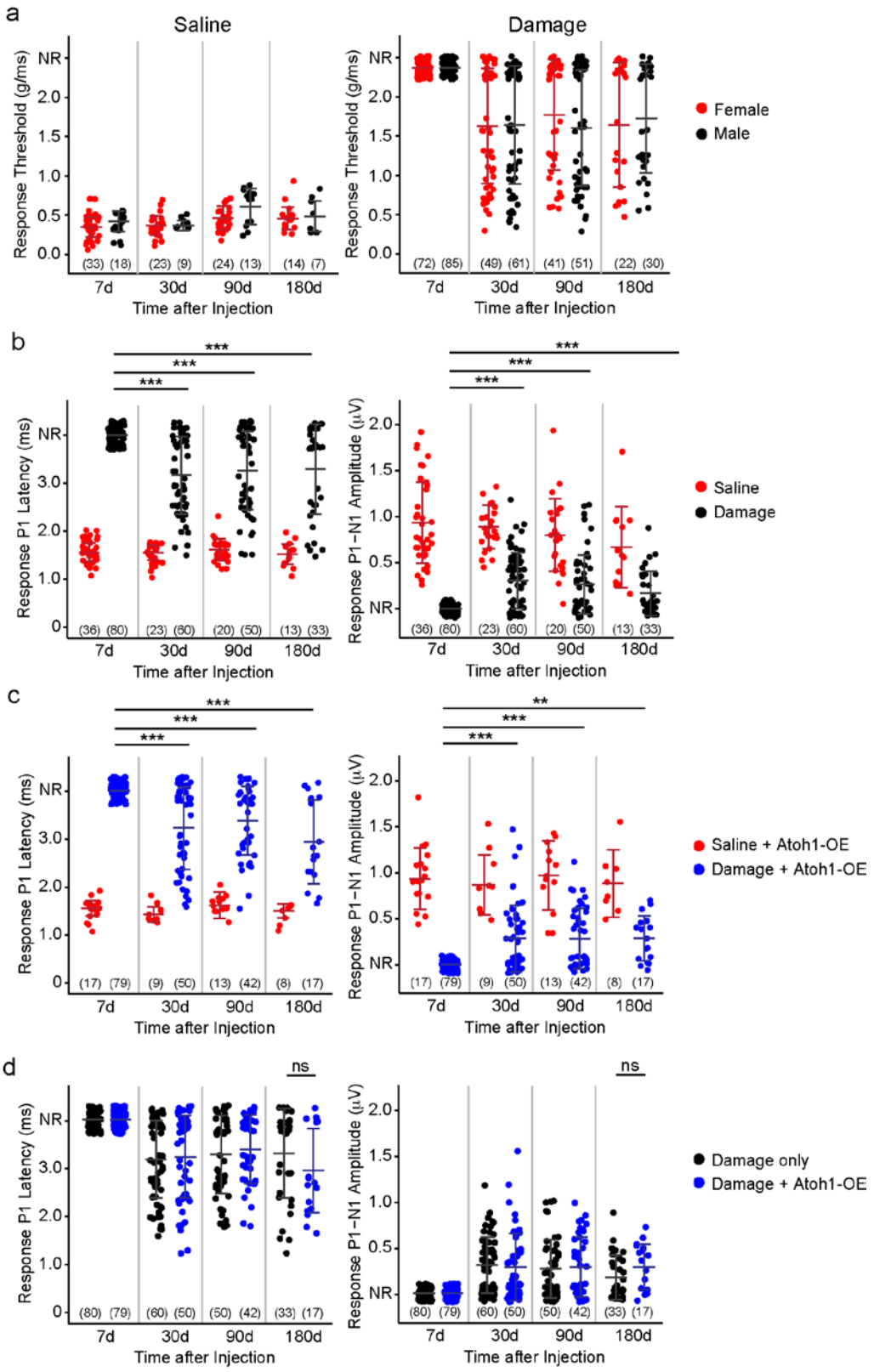
a
Saline
Damage
Response Threshold (g/ms)
NR
2.0
1.5
1.0
0.5
0.0
(33) (18)
(23) (9)
(24) (13)
(14) (7)
(72) (85)
(49) (61)
(41) (51)
(22) (30)
7d
30d
90d
180d
Time after Injection
Female
Male
b
***
***
***
Response P1 Latency (ms)
3.0
2.0
1.0
0
(36) (80)
(23) (60)
(20) (50)
(13) (33)
Response P1−N1 Amplitude (μV)
Saline
Damage
c
**
Saline + Atoh1-OE
Damage + Atoh1-OE
(17) (79)
(9) (50)
(13) (42)
(8) (17)
d
ns
Damage only
Damage + Atoh1-OE
(80) (79)
(60) (50)
(50) (42)
(33) (17)

Supplemental Figure 7. Functional recovery of the damaged, mature mouse utricle (related to Figure 5). (a) No sex differences of VsEP thresholds were found in saline-treated or IDPN-treated mice across all time points examined. (b) As a group, VsEP latencies and amplitudes of damaged-only animals significantly improved over time relative to seven days post damage (black). Latencies and amplitudes of undamaged animals were stable over multiple time points (red). (c) As a group, VsEP latencies and amplitudes of Atoh1 OE, damaged animals significantly improved over time relative to seven days post damage (blue). Latencies and amplitudes of Atoh1 OE, undamaged animals were stable over multiple time points (red). (d) In comparison to damage-only animals (black), VsEP latencies and amplitudes of Atoh1 OE, damaged animals (blue) were not significantly different across all time points examined. Two-way ANOVA with Tukey's multiple comparisons test, n for animals.

Figure S8

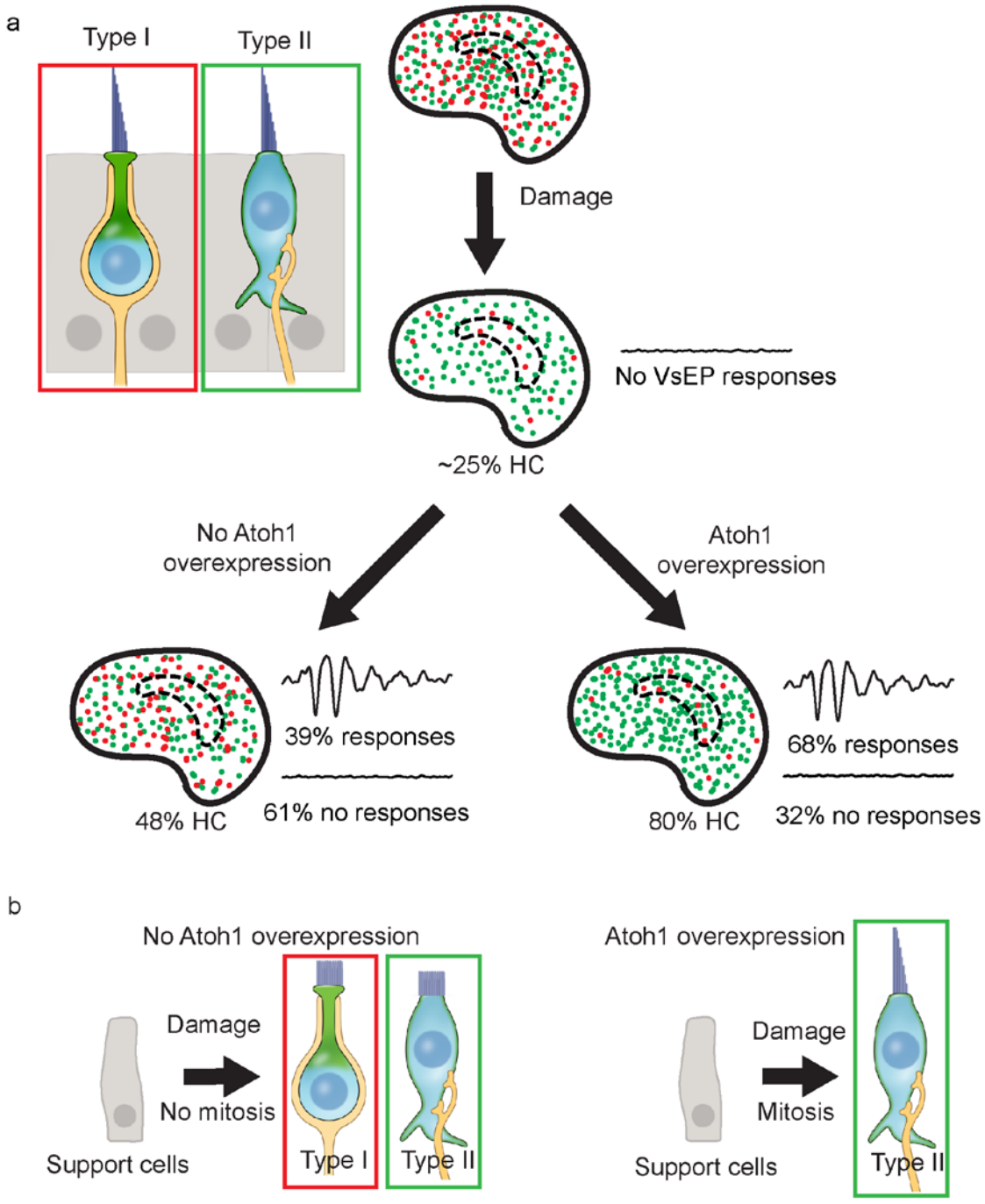

Supplemental Figure 8. Proposed mechanisms of Atoh1 OE in augmenting hair cell regeneration and recovery of vestibular physiology (related to Figures 1-5). (a) Treatment with IDPN results in significant loss of utricular HCs to ~25% of normal seven

days later, with mostly type II HCs remaining. Functionally, this results in a complete loss of VsEP waveforms. 180 days later, the adult mouse utricle regenerates type I and type II HCs—primarily in the extrastriolar region—to 48% of control levels, resulting in a sustained recovery of VsEP waveforms in 39% of mice. 180 days after IDPN-induced damage and Atoh1 OE, total HC number increased to 80% of age-matched control levels, with mostly type II HCs regenerated in both the striolar and extrastriolar regions. Functionally, 68% of IDPN-treated, Atoh1-overexpressed mice have a sustained recovery of VsEP function. (b) After damage only, support cells of the spontaneously regenerating adult mouse utricle differentiate into type I and type II HCs through non-mitotic mechanisms. After damage and Atoh1 OE, support cells proliferate and also regenerate type II HCs with elongated stereocilia and innervation.

Supplemental Table 1. Quantification of Myosin7a$^+$ hair cells (related to Figure 2).

Supplemental Table 1. Quantification of Myosin7a$^+$ hair cells

Extrastriola					
	Time after injection	No damage	Atoh1 OE only	Damage	Damage + Atoh1 OE
Total cells	7 days	182.4±41.9$^{\#\#\#}$ (9)	161.4±39.3$^{\#\#\#}$ (6)	53.5±24.7 (20)	63.2±24.9 (15)
	30 days	188.7±31.2$^{\#\#\#}$ (10)	208.7±41.4$^{\#\#\#}$ (3)	83.1±17.0 (16)	84.2±16.8 (6)
	90 days	159.6±37.9 (7)	199.3±47.0 (3)	89.2±28.5* (24)	108.4±23.8 (5)
	180 days	167.6±37.4 (11)	159.0±15.2 (4)	95.2±25.8$^{***,\#\#\#}$ (35)	144.8±39.2*** (19)
HA$^+$ cells	7 days	0.2±0.4 (5)	1.3±1.2 (3)	0.3±0.8 (7)	10.8±4.3 (8)
	30 days	0.0±0.0 (3)	1.7±1.2 (3)	3.0±4.2 (5)	16.2±11.9 (5)
	90 days	0.0±0.0$^{\#\#\#}$ (5)	2.3±1.5$^{\#\#}$ (3)	0.0±0.0$^{\#\#\#}$ (5)	46.3±28.5** (4)
	180 days	1.3±1.9$^{\#\#\#}$ (7)	5.3±3.1$^{\#\#\#}$ (3)	1.0±1.1$^{\#\#\#}$ (8)	81.4±36.3*** (7)
Striola					
	Time after injection	No damage	Atoh1 OE only	Damage	Damage + Atoh1 OE
Total cells	7 days	162.8±42.3$^{\#\#\#}$ (9)	135.3±43.2$^{\#\#\#}$ (6)	51.1±18.9 (20)	48.6±24.1 (15)
	30 days	159.3±45.8$^{\#\#\#}$ (10)	192.8±28.7$^{\#\#\#}$ (3)	71.2±18.8 (16)	79.5±18.3 (6)
	90 days	150.1±47.6 (7)	155.3±14.6 (3)	68.0±27.7 (24)	97.2±7.1 (5)
	180 days	149.9±36.4$^{\#\#}$ (11)	145.5±34.0 (4)	69.1±25.7$^{\#}$ (35)	100.8±36.2*** (19)
HA$^+$ cells	7 days	0.2±0.4 (5)	1.7±1.5 (3)	0.0±0.0 (7)	6.1±5.6 (8)
	30 days	0.0±0.0 (3)	1.0±1.0 (3)	0.0±0.0 (5)	13.2±8.0 (5)
	90 days	0.2±0.4$^{\#\#\#}$ (5)	1.3±0.6$^{\#\#}$ (3)	0.0±0.0$^{\#\#}$ (5)	37.0±23.9*** (4)
	180 days	0.6±1.0$^{\#\#\#}$ (7)	2.7±1.2$^{\#\#\#}$ (3)	2.0±4.9$^{\#\#\#}$ (8)	53.6±25.8*** (7)

Shown are Myosin7a$^+$ hair cell counts as well as Myosin7a$^+$ HA$^+$ hair cells per 10,000 µm^2 from 7, 30, 90, and 180 days after treatment. Mean ± SD. Number of animals listed in parentheses.

* Represents significant difference with respect to the 7-day time point within a damage group.

Represents significant difference within the same time point between damaged + Atoh1-OE and the other groups.

* p<0.05, ** p<0.01, *** p<0.001 (two-way ANOVA followed by post-hoc analysis via Tukey's multiple comparisons test).

$^{\#}$ p<0.05, $^{\#\#}$ p<0.01, $^{\#\#\#}$ p<0.001 (two-way ANOVA followed by post-hoc analysis via Tukey's multiple comparisons test).

Supplemental Table 2. Quantification of HA$^+$ hair cells

Extrastriola				
	Days post damage	Damage alone	Damage + Atoh1 OE (1 dose)	Damage + Atoh1 OE (2 doses)
Total hair cells	7 days	53.5±24.7 (20)	70.6±23.9 (8)	63.2±24.9 (15)
	30 days	83.1±17.0 (16)	88.8±16.5 (5)	84.2±16.8 (6)
	90 days	89.2±28.5** (24)	112.1±14.1 (8)	108.4±23.8 (5)
	180 days	95.2±25.8** (35)	115.9±34.1*** (7)	144.8±39.2***,### (19)
HA$^+$ hair cells	7 days	0.3±0.8 (7)	6.3±7.9 (11)	10.8±4.3 (8)
	30 days	3.0±4.2 (5)	10.6±11.3 (5)	16.2±11.9 (5)
	90 days	0.0±0.0 (5)	22.8±20.3 (11)	46.3±28.5## (4)
	180 days	1.0±1.1 (8)	16.6±26.0 (10)	81.4±36.3***,### (7)
Striola				
	Days post damage	Damage alone	Damage + Atoh1 OE (1 dose)	Damage + Atoh1 OE (2 doses)
Total hair cells	7 days	51.1±18.9 (20)	57.3±17.6 (10)	48.6±24.1 (15)
	30 days	71.2±18.8 (16)	78.6±29.0 (5)	79.5±18.3 (6)
	90 days	68.0±27.7 (24)	80.4±17.6 (11)	97.2±7.1 (5)*
	180 days	69.1±25.7 (35)	74.2±30.2 (10)	100.8±36.2***,## (19)
HA$^+$ hair cells	7 days	0.0±0.0 (7)	6.3±11.7 (11)	6.1±5.6 (8)
	30 days	0.0±0.0 (5)	7.8±4.3 (4)	13.2±8.0 (5)
	90 days	0.0±0.0 (5)	8.0±6.2 (11)	37.0±23.9 (4)**,##
	180 days	2.0±4.9 (8)	11.4±18.2 (10)	53.6±25.8 (7)***,###

Shown are Myosin7a$^+$ hair cell counts as well as Myosin7a$^+$ HA$^+$ hair cells per 10,000 µm^2 from 7, 30, 90, and 180 days after IDPN-induced damage. Mean ± SD. Number of animals listed in parentheses.

* Represents significant difference across time points within a damage group between 7 days and later time points.

Represents significant difference within 1 time point between damage alone and other groups.

* p<0.05, ** p<0.01, *** p<0.001 (two-way ANOVA followed by post-hoc analysis via Tukey's multiple comparisons test).

p<0.01, ### p<0.001 (two-way ANOVA followed by post-hoc analysis via Tukey's multiple comparisons test).

Supplemental Table 2. Quantification of HA$^+$ hair cells (related to Figure 2).

Supplemental Table 3. Quantification of proliferating cells in the mature mouse utricle (related to Figure 2).

Supplemental Table 3. Quantification of proliferating cells in the mature mouse utricle

		Ki67		
	Time after injection	No damage	Atoh1 OE only	Damage only	Damage + Atoh1 OE
Hair cells	7 days	0.0±0.0 (5)	0.0±0.0 (3)	0.7±2.0 (9)	1.3±2.1 (10)
	30 days	0.0±0.0 (5)	0.0±0.0 (5)	0.0±0.0 (6)	0.1±0.3 (10)
	90 days	n/a	n/a	0.0±0.0 (3)	0.0±0.0 (4)
Support cells	7 days	0.0±0.0 (5)	0.0±0.0 (3)	0.0±0.0 (9)	0.1±0.3 (10)
	30 days	0.0±0.0 (5)	0.0±0.0 (5)	0.0±0.0 (6)	4.4±9.6 (10)
	90 days	n/a	n/a	0.0±0.0 (3)	0.0±0.0 (4)
		EdU			
	Time after injection	No damage	Atoh1 OE only	Damage only	Damage + Atoh1 OE
Hair cells	7 days	0.0±0.0 (3)	0.0±0.0 (3)	0.2±0.4 (5)	0.0±0.0 (6)
	30 days	0.0±0.0 (4)	0.2±0.4 (5)	0.0±0.0 (3)	1.5±4.1 (19)
	90 days	n/a	n/a	0.0±0.0 (4)	1.5±3.0 (4)
Support cells	7 days	0.0±0.0 (3)	0.0±0.0 (3)	0.0±0.0 (5)	0.0±0.0 (6)
	30 days	0.0±0.0 (4)	0.0±0.0 (5)	0.0±0.0 (3)	20.9±37.3 (19)
	90 days	n/a	n/a	0.8±1.5 (4)	15.8±28.9 (4)

Shown are $Ki67^+$ and EdU^+ hair cell and support cell counts per utricle from 7, 30, and 90 days after treatment. Mean ± SD. Number of animals listed in parentheses.

Supplemental Table 4. Physiology of the damaged and regenerating mouse utricle (related to Figure 5).

Supplemental Table 4. Physiology of the damaged and regenerating mouse utricle

Spontaneous				
Time after injection	Control (11)	Sustained recovery (11)	Unsustained recovery (13)	No recovery (5)
7 days	0.35±0.11	NR	NR	NR
30 days	0.39±0.14	1.32±0.76	1.56±0.76	NR
90 days	0.44±0.12	1.60±0.79	1.73±0.54	NR
180 days	0.52±0.18	1.08±0.29	NR	NR
Atoh1 OE				
Time after injection	Control (5)	Sustained recovery (13)	Unsustained recovery (2)	No recovery (4)
7 days	0.42±0.17	NR	NR	NR
30 days	0.37±0.07	1.84±0.75	2.03±0.49	NR
90 days	0.69±0.13	1.72±0.78	1.19±0.00	NR
180 days	0.44±0.15	0.89±0.37	NR	NR

Shown are average VsEP response thresholds (g/ms) from various recovery groups from 7, 30, 90, and 180 days after saline-treated and IDPN-induced damage. Mean ± SD. Number of animals listed in parentheses.